Geophys. J. Int. (2009) **178,** 419–446 doi: 10.1111/j.1365-246X.2009.04153.x

Seismic interferometry of scattered surface waves in attenuative media

David Halliday[1,2] and Andrew Curtis[1,2]

[1]*School of GeoSciences, Grant Institute, Kings Buildings, University of Edinburgh, West Mains Road, Edinburgh,* EH93JW*, United Kingdom.*
E-mail: d.f.halliday@sms.ed.ac.uk
[2]*Edinburgh Collaborative of Subsurface Science and Engineering (ECOSSE), Edinburgh, United Kingdom*

Accepted 2009 February 10. Received 2009 February 5; in original form 2008 July 11

SUMMARY

Seismic interferometry can be used to estimate interreceiver surface wave signals by cross-correlation of signals recorded at each receiver that are emitted from a surrounding boundary of impulsive or uncorrelated noise sources. We study seismic interferometry for scattered surface waves using a stationary-phase analysis and surface wave Green's functions for isotropic point scatterers embedded in laterally homogeneous media. Our analysis reveals key differences between the interferometric construction of reflected and point-scattered body or surface waves, since point scatterers radiate energy in all directions but a reflection from a finite flat reflector is specular. In the case of surface waves, we find that additional cancelling terms are introduced in the stationary-phase analysis for scattered waves related to the constraint imposed by the optical theorem for surface waves. The additional terms are of second order even for single-scattered waves, and we show that these can be highly significant in multiple-scattering cases. In attenuative media errors are introduced due to amplitude errors in these additional terms. Further, we find that as the distribution of scatterers in a medium becomes more complex the errors in correlation-type interferometry caused by attenuation in the background medium become larger. Convolution-type interferometry has been shown to be effective when considering electromagnetic wavefields in lossy media, and we show that this is also true for scattered surface waves in attenuating elastic media. By adapting our stationary-phase approach to this case, we reveal why convolution-type interferometry performs well in such media: the second-order cancelling terms that appear in the correlation-type approach do not appear in convolution-type interferometry. Finally, we find that when using both correlation- and convolution-type interferometry with realistic source geometries (illustrative of both industrial seismics and 'passive noise' interferometry), we cannot necessarily expect to produce estimates with all dominant scattering events present. This is shown to be especially important if, as proposed previously for electromagnetic applications, the convolution and correlation approaches are compared to help identify errors in the interferometric estimates.

Key words: Interferometry; Surface waves and free oscillations; Theoretical seismology; Wave scattering and diffraction.

1 INTRODUCTION

Seismic interferometry loosely refers to a range of methods, within which interreceiver seismograms are estimated by cross-correlation and summation of wavefields recorded at each receiver (Claerbout 1968; Lobkis & Weaver 2001; Weaver & Lobkis 2001; Campillo & Paul 2003; Shapiro & Campillo 2004; Snieder 2004b; Wapenaar 2004). The ability to create estimates of interreceiver surface waves by seismic interferometry is of great interest to seismologists: since passive noise sources tend to occur near the Earth's surface, interreceiver surface wave estimates can be constructed from noise recordings and can be used to create velocity maps or profiles in global or regional seismology (Shapiro & Campillo 2004; Shapiro *et al.* 2005; Gertstoft *et al.* 2006; Moschetti *et al.* 2007; Yang *et al.* 2007). Such studies focus on group-velocity traveltime tomography and extract only fundamental-mode surface wave information since this mode is synthesized relatively easily using background noise. However, by analysing the errors that occur specifically when attempting to extract higher-mode surface wave information from interferometry using only near-surface sources, Halliday & Curtis (2008) proposed a method to measure interreceiver, direct, higher-mode surface waves robustly.

Actively induced source signals can also be cross-correlated to synthesize interreceiver surface wave estimates, for example, Halliday *et al.* (2008) demonstrate that it is possible to recover higher-mode interreceiver surface waves using specific geometries as predicted by Halliday & Curtis (2008). Curtis *et al*. (2006), Dong *et al*. (2006) and Halliday *et al*. (2007) propose that similar interreceiver surface wave estimates can be used as part of a ground-roll (surface-wave) removal method in exploration seismology.

In addition to direct, interreceiver surface waves, in many cases, it may be desirable to recover scattered surface waves using interferometry, since these contain additional information about near-surface heterogeneities (Snieder 1986; Snieder & Nolet 1987; Levander 1990). In Rayleigh-wave tomography, it is important to consider scattering effects when significant heterogeneities exist on length scales comparable to the wavelength of seismic waves or to the width of Fresnel zones, as ray theory tends to break down in such circumstances (e.g. Spetzler & Snieder 2001). This has prompted many different (non-interferometric) studies of surface wave scattering. For example, Snieder (1986) and Snieder & Nolet (1987) developed a theoretical framework for analysing scattered surface waves and employed the Born (single-scattering) approximation to construct an inversion scheme that identified strong crustal-scale surface wave scatterers, such as mountain roots. Further single-scattering methods are proposed by Meier *et al.* (1997), Marquering *et al.* (1999), Spetzler *et al.* (2002) and Ritzwoller *et al.* (2002). When compared with ray theoretical approaches, these methods often find significant differences in imaged features. For example, Ritzwoller *et al.* (2002) find that by using a single-scattering approach (so-called diffraction tomography), larger velocity anomalies and deeper mantle features can be identified. Thus, if scattered surface waves can be recovered by seismic interferometry, the power and applicability of the method to crustal seismology may be greatly increased.

Scattered surface waves are also observed in higher-frequency near-surface settings. For example, in engineering seismology higher-frequency scattered surface waves can be used to image the near-surface properties of the Earth (e.g. Herman *et al.* 2000; Campman & Riyanti 2007; Kaslilar 2007). In exploration seismology, similar high-frequency scattered surface waves are of interest for an altogether different reason. Surface wave (or ground-roll) signals, in general, provide little useful information in exploration seismology, as they mask other more useful body wave arrivals and hence are regarded as noise. Lateral scattering in the near-surface of the Earth results in a form of surface wave noise that is particularly difficult to remove, since its time-varying directions of arrival are unknown *a priori*. Several algorithms have been proposed to remove the scattered surface waves (Blonk *et al.* 1995; Blonk & Herman 1996; Ernst *et al.* 2002a,b; Campman *et al.* 2005; Campman *et al.* 2006; Herman & Perkins 2006). Such algorithms rely on single-scattering approximations, inverse-scattering schemes and forward modelling (with the exception of Herman & Perkins (2006) who use a data-driven inversion approach). Acquisition-based suppression schemes also exist, in which arrays are used to suppress near-surface scattering (Morse & Hildebrandt 1989; Regone 1998; Özbek 2000a,b). However, the spatial resolution of the data may be compromized by using spatially extensive arrays, and as the exploration seismics industry moves towards so-called point-receiver (i.e. single-sensor, rather than stacked-array) recordings, new algorithms may be required to suppress noise.

The application of interferometry to ground-roll removal is of particular interest, because interferometry is naturally applied directly to point-receiver recordings. It provides the potential to synthesize complex scattered surface wave fields without approximations, no forward modelling or inversion is required; and it is entirely data driven. The potential downside is that the use of many cross-correlation operations and least-squares filtering for ground-roll removal (e.g. Dong *et al.* 2006; Halliday *et al.* 2007) may make the method more costly computationally than more conventional (and in some cases ineffective) methods of ground-roll removal such as frequency–wavenumber (f–k) or frequency–offset (f–x) domain methods.

From this wide range of applications, it is clear that the recovery of scattered surface waves using interferometry could be of great benefit to a range of methods in seismology. Scattered surface waves have been recovered in ultrasonic lab experiments, for example, Malcolm *et al.* (2004) recover estimates of the Rayleigh-wave Green's function in a strongly scattering diffusive regime. However, a successful application for seismic scattered surface waves has yet to be published. There are several possible reasons for this, including poor source coverage and the weak strength of scattered waves relative to errors in the interferometric estimates, or it could simply be that these arrivals are not being sought—without arrays of seismometers, it is difficult to identify fundamental, higher-mode and scattered surface waves unambiguously.

For correlation-type interferometry to produce exact, interreceiver Green's functions, there are a number of conditions that must be met, including that the medium is non-attenuating, and that there exists a closed boundary of 'background' noise sources of both the unidirectional point force and deformation-rate-tensor types (Wapenaar 2004; van Manen *et al.* 2005; van Manen *et al.* 2006; Wapenaar & Fokkema 2006). However, note first that in reality the near surface often exhibits very strong attenuation, and second that it is by relaxing the conditions on boundary sources that we observe a dominance of surface waves (Shapiro *et al.* 2005; Halliday *et al.* 2007). Hence, to apply interferometry to scattered surface waves successfully, we must first understand characteristics of the method in non-ideal circumstances.

In exploration applications, similar relaxation of these conditions are forced upon us. For example, sources are often restricted to the surface of the Earth and only vertical point-force sources may be available. Nevertheless, in certain cases, there are methods with which resulting errors in the interferometric results can be suppressed. For example, in the virtual-source method of Bakulin & Calvert (2004, 2006), the stationary-phase work of Snieder *et al.* (2006) illustrates a source of spurious arrivals (any non-physical arrival in the interferometric estimates that does not correspond to an actual interreceiver event) in the simple case of a two half-space model, and Mehta *et al.* (2007) use wavefield separation to suppress the effect of spurious arrivals.

In an earlier paper (Halliday & Curtis 2008), we use a similar stationary phase approach to Snieder (2004a,b) and Snieder *et al.* (2006) to investigate the effects of relaxing conditions on the surrounding boundary for the case of direct, multi-mode surface waves, illustrating the effectiveness of various depleted background noise-source geometries and the errors that occur in such cases in the presence of higher-mode direct surface waves. In Halliday & Curtis (2009), we extend this approach for scattered surface waves to derive a generalized optical theorem for surface waves. In this paper, a stationary-phase evaluation reveals the steps involved in interferometric estimation of scattered surface waves. We find that there are key differences between the stationary-phase analysis of interferometry for reflected and scattered waves that are accounted for by considering second-order terms in the interferometric integral, even for single-scattered waves. This suggests that a first-order Born approximation is not suitable to analyse the effect of interferometry on scattered waves (and since our approach can be applied to general scattering of waves, this observation applies not only to surface waves but to different wave types, e.g. see Snieder *et al.* 2008).

We find that errors in the cross-correlation approach are sensitive to attenuation and limited aperture. Convolution-type interferometry is an adaptation of interferometric theory that allows for the

presence of attenuation (Slob *et al.* 2007; Slob & Wapenaar 2007). By adapting our stationary-phase approach for the convolution case, we identify why interferometry performs better in that case: mutually cancelling terms identified in the correlation approach do not exist in convolution-type interferometry. In addition to the expected improvements in the presence of attenuation, this also suggests that convolution-type interferometry is less sensitive to non-physical arrivals introduced by limited aperture (e.g. an incomplete boundary of sources, or boundary sources of significantly diminished magnitude over some set of locations). Slob *et al.* (2007) propose combining correlation- and convolution-type interferometry to identify non-physical errors in electromagnetic wavefield estimates, and likewise, we may consider a similar approach in the scattered surface wave case. However, by considering realistic geometries we find that certain geometries may not produce estimates containing all dominant scattered surface waves in either or both cases. Hence, if we wish to use a combined approach, we must be careful as scattered surface waves could be incorrectly identified as spurious arrivals. Results and discussions are illustrated throughout using semi-analytical, scattered surface wave examples.

We first discuss stationary points on a closed boundary of 'background' noise sources for the interferometric synthesis of scattered surface waves, explaining how interferometry works for scattered surface waves (leaving mathematical derivations to appendices). We then investigate the effect of attenuation on the recovery of scattered surface waves, showing how spurious arrivals are introduced in this case. By using an adaptation of the convolution approach of Slob *et al.* (2007) and Slob & Wapenaar (2007) for elastic surface waves, we adapt our stationary-phase analysis to identify why scattered surface waves are better estimated using this approach (note that Wapenaar 2007 also derives convolution-type interferometric relationships for the general case of diffusion, flow and wave phenomena). Finally, we combine the effects of realistic source geometries with the use of only point-force sources in an attenuating medium, illustrating the sensitivities of the two approaches to non-physical arrivals introduced by attenuation and limited aperture.

In Appendix A, we summarize the stationary-phase analysis for scattered surface waves presented by Halliday & Curtis (2009). Although the initial part of this analysis is similar to the work on reflected body-waves of Snieder *et al.* (2006), our analysis reveals key differences between the reflected body wave case and the scattered surface wave case (and this analysis can be generalized to reveal differences between reflected and scattered waves for other wave types). These differences are resolved only by using an optical theorem for scattered surface waves. Halliday & Curtis (2009) derive a generalized optical theorem for surface waves, and here we consider the special case of scattering due to a symmetric, isotropic, density perturbation. This is considered in the final part of Appendix A, where we derive the necessary constraints on the real and imaginary parts of the surface-wave scattering amplitude for an isotropic density perturbation.

In Appendix B, we discuss aspects of changes that occur when we consider convolution-type interferometry in place of correlation-type interferometry and illustrate where errors may be introduced in that case.

2 STATIONARY PHASE ANALYSIS FOR SCATTERED SURFACE WAVES

Seismic interferometry is applied by solving a so-called interferometric integral, of which there are many forms, depending on factors such as quantities radiated and measured by sources and receivers,

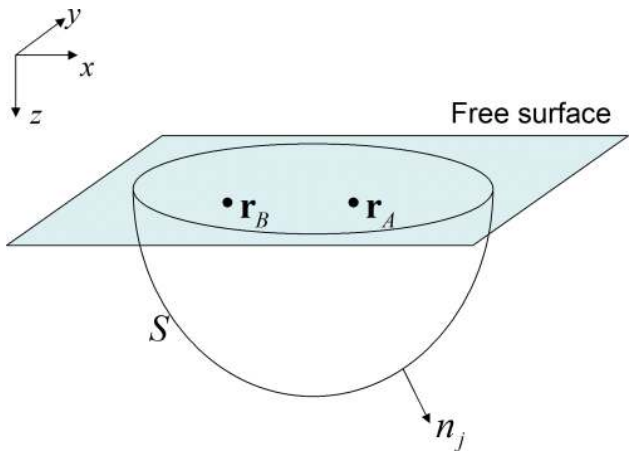

Figure 1. Geometry for eq. (1). Note that $\mathbf{r}_A$ and $\mathbf{r}_B$ lie beneath the free surface in this case.

respectively, and the type of media considered, for example, for acoustic wavefields (Wapenaar 2004; van Manen *et al.* 2005), for elastic wavefields (van Manen *et al.* 2006; Wapenaar & Fokkema 2006) and for electromagnetic wavefields (Slob & Wapenaar 2007). We use an integral describing the extraction of particle displacement, point-force source Green's functions in elastic media (van Manen *et al.* 2006):

$$G^*_{im}(\mathbf{r}_B, \mathbf{r}_A) - G_{im}(\mathbf{r}_B, \mathbf{r}_A) = \int_{\mathbf{r}_S \in S} \left\{ G_{in}(\mathbf{r}_B, \mathbf{r}_S) n_j c_{njkl} \partial_k G^*_{ml}(\mathbf{r}_A, \mathbf{r}_S) - n_j c_{njkl} \partial_k G_{il}(\mathbf{r}_B, \mathbf{r}_S) G^*_{mn}(\mathbf{r}_A, \mathbf{r}_S) \right\} \mathrm{d}S, \quad (1)$$

where $G_{im}(\mathbf{r}_B, \mathbf{r}_A)$ denotes the Green's function representing the ith component of particle displacement at location $\mathbf{r}_B$ due to a uni-directional, impulsive, point force in the m direction at $\mathbf{r}_A$, $\partial_k G_{ml}(\mathbf{r}_A, \mathbf{r}_S)$ is the spatial partial derivative at location $\mathbf{r}_S$, taken in the k direction of the Green's function $G_{ml}(\mathbf{r}_A, \mathbf{r}_S)$, c_{njkl} is the elasticity tensor, superscript * denotes complex conjugation and n_j is the outward normal to the arbitrarily shaped closed surface S, where S encloses the locations $\mathbf{r}_A$ and $\mathbf{r}_B$ (e.g. see Fig. 1). Einstein's summation convention applies for repeat indices. The term $n_j c_{njkl} \partial_k G_{ml}(\mathbf{r}_A, \mathbf{r}_S)$ represents the particle displacement at $\mathbf{r}_A$ due to a deformation-rate-tensor source at $\mathbf{r}_S$.

We use the method of stationary-phase integration to evaluate the integral in eq. (1), using scattered surface wave Green's functions (e.g. see Snieder (2002) and eqs A1–A5 in Appendix A). This method assumes that the dominant contribution to the integral comes from locations on the integration boundary, where the phase of the integrand becomes stationary with respect to locations on the boundary, and that the amplitude of the term being integrated varies slowly around this location (Snieder 2004a). This is a useful tool for analysing the processes and approximations involved in seismic interferometry. By using analytical Green's functions, we can determine the conditions where the integral is stationary and evaluate the contribution from such points explicitly.

For example, Snieder (2004b) uses the stationary-phase approximation to demonstrate that a homogeneous distribution of scatterers, acting as secondary wavefield sources, could be used to estimate interreceiver, direct, ballistic waves and applies the same approach to the special case of interreceiver surface waves. Snieder *et al.* (2006) use the stationary-phase approximation to evaluate the interferometric integral for reflected body wave fields when using only Earth surface sources (i.e. a truncated surface, S) and find a

significant source of error that occurs in the form of 'spurious multiples'. Independently, Sabra *et al.* (2005) applied a similar approach but for acoustic guided waves, illustrating that guided-wave stationary points exist at a range of offsets throughout a waveguide.

Halliday & Curtis (2008) extend the approach of Snieder (2004b) for direct surface waves to illustrate the adverse effects of limited surface source geometry, especially in the presence of higher-mode surface waves. Here we take this approach one step further and consider scattered surface waves. In what follows, we assume that steps have been taken to treat higher-mode surface waves correctly: using only surface sources, non-physical cross-mode correlation terms are introduced into the interferometric estimate in the presence of multiple surface wave modes; by separating modes prior to interferometry, these cross-mode terms are suppressed.

2.1 Single scattered surface waves

The stationary-phase evaluation is lengthy and, in some places, mirrors the approaches of Snieder (2004b), Snieder *et al.* (2006) and Halliday & Curtis (2008). In Appendix A, we show that there are four different stationary-phase contributions to the interferometric estimation. This is similar to the analysis of reflected body waves by Snieder *et al.* (2006). However, we find that in the scattering case, there are additional contributions to interferometry that do not appear in the approach of Snieder *et al.* (2006). To account for these differences, we consider the optical theorem for surface waves (Snieder 1988; Brandenburg & Snieder 1989; Halliday & Curtis 2009). We now discuss each of these stationary phase contributions and illustrate them both graphically and synthetically.

The four different contributions (*T1–T4*) to the interferometric integral are: the cross-correlation of the direct surface waves recorded at each receiver (*T1*); the cross-correlation of the direct surface wave at receiver one with the scattered surface waves at receiver two (*T2*); the cross-correlation of the scattered surface wave at receiver one with the direct surface wave at receiver two (*T3*) and the cross-correlation of the scattered surface waves at both receivers (*T4*). Provided that multiple surface wave modes are properly dealt with (as discussed above), we can consider that this analysis holds for sources distributed only at (or just beneath) the surface of the Earth, with the introduction of some frequency-dependent scale factors (see Halliday & Curtis 2008).

Snieder *et al.* (2006) find that the cross-correlation of two direct body waves results in the recovery of the direct interreceiver body wave. Likewise, the cross-correlation of the direct surface waves (*T1*) results in the recovery of the direct interreceiver surface waves. This part of the integral is similar to the case discussed by Snieder (2004b) and is the same as that discussed by Halliday & Curtis (2008), and we refer the reader to those studies for a more detailed analysis.

T2 and *T3* are similar to the cross-correlation of the direct and reflected body waves in Snieder *et al.* (2006). They find that one term provides the causal reflected body wave and the other provides the acausal reflected body wave. Similarly, we find that *T2* and *T3* provide the causal and acausal interreceiver scattered surface wave.

However, our analysis reveals a difference between the previous approach of Snieder *et al.* (2006) for singly reflected body waves and that for scattered surface waves: in addition to these physical terms (eqs A27 and A29 in Appendix A), there are also non-physical terms associated with *T2* and *T3*, which are introduced in the case of scattered waves (eqs A28 and A30 in Appendix A). Such non-physical terms are often referred to as spurious arrivals and have previously been observed in applications of interferometry in the presence of multiple reflections, where source distribution is insufficient, the recording time is not long enough and in the presence of losses (Snieder *et al.* 2006; Draganov *et al.* 2008; Ruigrok *et al.* 2008). In the lossless case, these arrivals are destructively cancelled by including the second-order term *T4*. Thus, we highlight general differences between the stationary-phase treatments of reflected and scattered wavefields in seismic interferometry. In an independent study, Snieder *et al.* (2008) derive similar results for acoustic-wave scattering; hence we expect analogous results to hold for other scattering regimes.

The differences between the stationary-phase analysis for reflected and scattered waves might seem counter-intuitive: since a plane reflector could be modelled as a line of scatterers separated within the Nyquist spatial-sampling criteria, it could be argued that the two cases should be interrelated. However, the key difference is that for a plane reflector, there is a single angle of reflection for any given angle of incidence. For an isolated point scatterer, waves are scattered over 360° for any angle of incidence. This affects the manner in which these waves are observed for different source–receiver configurations. We illustrate this difference in Fig. 2. Fig. 2(a) illustrates ray paths of waves from two source locations (s_1 and s_2), reflected at a plane reflector (z_0) and recorded at a single receiver (r_1). The azimuths of the incident and reflected waves and the position of the specular-reflection point changes with source position. Fig. 2(b) illustrates the same case, but the reflector has been replaced by a single point scatterer (z_0). For the different source locations, the azimuths of the incident wave changes, but the azimuth of the scattered wave does not, as the scatterer–receiver path is the same (i.e. is stationary) for all source locations. This is why we see differences between the cases for reflected and scattered waves.

We now discuss the contribution of *T2* and *T3* in more detail (geometric variables used to define these stationary points are illustrated in Fig. 3). In Appendix A, we find the stationary phase condition for scattered waves given by *T2* to be $\varphi_{S0} - \varphi_{A0} = 0$ and $\varphi_{S0} - \varphi_{A0} = \pi$ (or $\varphi_{S0} - \varphi_{B0} = 0$ and $\varphi_{S0} - \varphi_{B0} = \pi$ for *T3*). In Fig. 4, we illustrate the geometries associated with these conditions. Figs 4(a) and (b) illustrate what we will call the physical and non-physical parts of *T2,* respectively. For the physical part, we see that since both the direct and scattered waves have the same take-off angle ($\varphi = \varphi_{A0} = \varphi_{S0}$), the initial parts of both waves have the same path (i.e. this corresponds to the stationary condition $\varphi_{S0} - \varphi_{A0} = 0$). Interferometric cross-correlation acts to remove the time delay between the boundary stationary point and the first receiver, resulting in an estimate of the wavefield as if the source had been at $\mathbf{r}_A$. The latter is, also, why the second part of *T2* is non-physical: in Fig. 4(b), we can see that both waves reach the scatterer before they reach $\mathbf{r}_A$ (corresponding to the stationary condition $\varphi_{S0} - \varphi_{A0} = \pi$). The time-delay between the stationary point and the scatterer is removed, resulting in a non-physical contribution corresponding to the cross-correlation of the direct waves between the scatterer and the two receiver locations. In Figs 4(c) and (d), we examine *T3* by reversing the roles of $\mathbf{r}_A$ and $\mathbf{r}_B$ and again find one physical stationary point and one non-physical stationary point (where by physical and non-physical stationary points, we refer to those stationary points providing a physical contribution and a non-physical contribution, respectively).

The contribution from the physical stationary point relating to *T3* has the negative phase of the physical part of *T2*; so, thus, we recover both causal and acausal scattered events. We find that the non-physical parts of *T2* and *T3* have equal phase. If the scattering amplitude is real (as in a first-order Born analysis), these terms

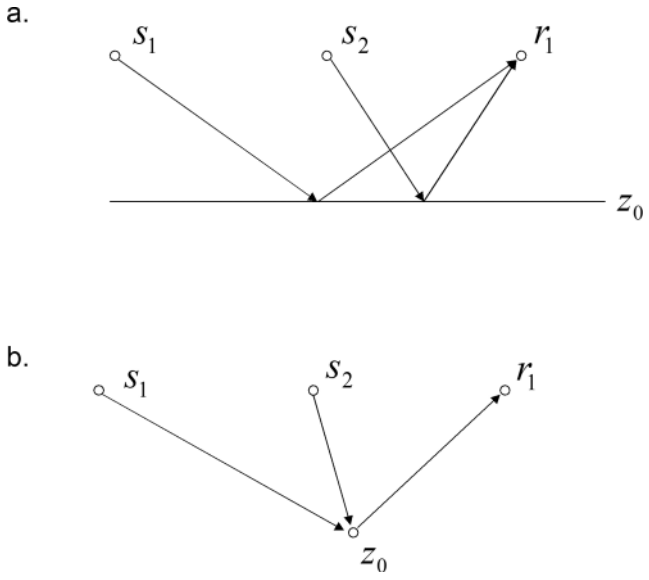

Figure 2. Sketch geometries illustrating the differences between reflected wavefields and scattered wavefields. Ray paths between two source locations (s_1 and s_2) and a receiver location (r_1) that have (a) been reflected by a planar interface (z_0) and (b) been scattered by a point scatterer (z_0).

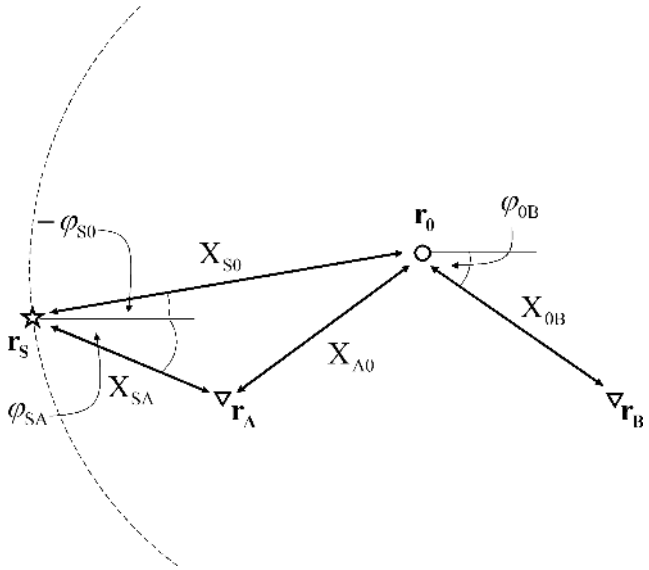

Figure 3. Definition of geometric variables required for terms *T2* and *T3* in the horizontal plane. Here we show the geometry of the direct surface wave at receiver location $\mathbf{r}_A$ due to a source at location $\mathbf{r}_S$, the horizontal projection of the source–receiver path length is X_{SA}; and the horizontal projection of the azimuth is φ_{SA}. The scattered wave is shown between source location $\mathbf{r}_S$ and receiver location $\mathbf{r}_B$, with the scatterer located at $\mathbf{r}_0$. The horizontal projection of the source-scatterer path is defined by length X_{S0} and angle φ_{S0} (shown as $-\varphi_{S0}$), and the horizontal projection of scatterer–receiver path is similarly defined by X_{0B} and φ_{0B}. Finally, we define the offset between $\mathbf{r}_A$ and $\mathbf{r}_0$ as X_{A0}.

have opposite sign and cancel mutually. However, if the scattering amplitude has an imaginary part, then the terms do not cancel (the imaginary parts have equal amplitude due to the complex conjugation in eq. 1). We now discuss why it is necessary to consider complex-scattering amplitude in any analysis, where we are interested in scattering beyond the Born approximation.

Term *T4* of Snieder *et al.* (2006) provides a stationary-phase contribution that corresponds to the acausal direct body wave. *T4* in our scattering analysis is altogether different, as it is always stationary: the scatterer does not move, hence the phase of the cross-correlation of the two scatterer-to-receiver waves remains constant (eq. A31 in Appendix A). The cross-correlation has the opposite phase to that of the non-physical parts of *T2* and *T3*, and the combination of these three terms must mutually cancel to zero. In Appendix A, we show that for this cancellation to occur, it is necessary to consider a complex scattering amplitude, and as a result of this analysis, we derive the constraints that the optical theorem places on surface wave scattering due to an isotropic density perturbation. We must therefore require that scattering be computed in a manner consistent with the optical theorem (Halliday & Curtis 2009 use a similar approach to derive a generalized optical theorem for surface waves, as opposed to the specific case of an isotropic density perturbation considered here). This indicates that linearized Born scattering (which is inconsistent with the optical theorem) does not produce the correct interferometric result, even in this simple single-scattering case. This is because the cross-correlation of two scattered waves can be considered a second-order term, and term *T4* would therefore not be considered in a Born analysis (that is, for real scattering amplitudes we would only consider terms *T2* and *T3*). Vasconcelos (2007) derives interferometric relations using representation theorems for perturbed media and finds similar results to our stationary phase approach. That approach is for general perturbations to the background medium in acoustic media and considers remote sensing applications of terms equivalent to *T2–T4* of our analysis. However, it did not identify the critical role of the imaginary part of the scattering amplitude.

We now illustrate the above results using synthetic data generated in a simple model with a boundary S of radius 200 m from the origin, on which the source separation is 4 m, a single scatterer at [50, 50] and receivers located internally at [−140, 0] and from [−16, 0] to [140, 0] in steps of 4 m (Fig. 5a). For illustrative purposes, we use both point-force sources and deformation-rate-tensor sources to be precisely consistent with the terms G_{in} and $n_j c_{njkl} \partial_k G_{il}$ in eq. (1), respectively (this also ensures that no amplitude errors are introduced due to far-field approximations, such as those discussed by Wapenaar & Fokkema (2006)). We also consider only a single surface wave mode (taken from the horizontally plane-layered earth model used by Halliday & Curtis 2008) with a frequency-dependent velocity range of approximately 100–160 ms^{-1} over the frequency band of interest (selected by using a Ricker wavelet with a centre frequency of 15 Hz). We therefore assume that we can consider a boundary of sources located only at (or just beneath) the surface of the Earth, and hence we expect frequency-dependent scaling terms due to the omission of sources at depth, as predicted by Halliday & Curtis (2008). We compute the data using eqs (A2)–(A5) in Appendix A. To produce strong scattering, we use the upper limit of these constraints imposed by the optical theorem on the imaginary and real parts of the scattering amplitude, as derived in Appendix A. The imaginary part of the non-azimuthally dependent scattering amplitude is set to −0.9, and the imaginary part of the azimuthally dependent scattering amplitude is set to −1.9.

In Fig. 6, we consider the receivers [−140, 0] and [120, 0]. Fig. 6(a) illustrates the cross-correlation and summation of the direct surface waves recorded at these two receivers from all boundary sources, and the exact direct surface wave is plotted for reference (dashed line). All plots are scaled to the maximum amplitude of this estimated direct surface wave. Fig. 6(b) illustrates the result of cross-correlating the direct surface waves with the scattered surface

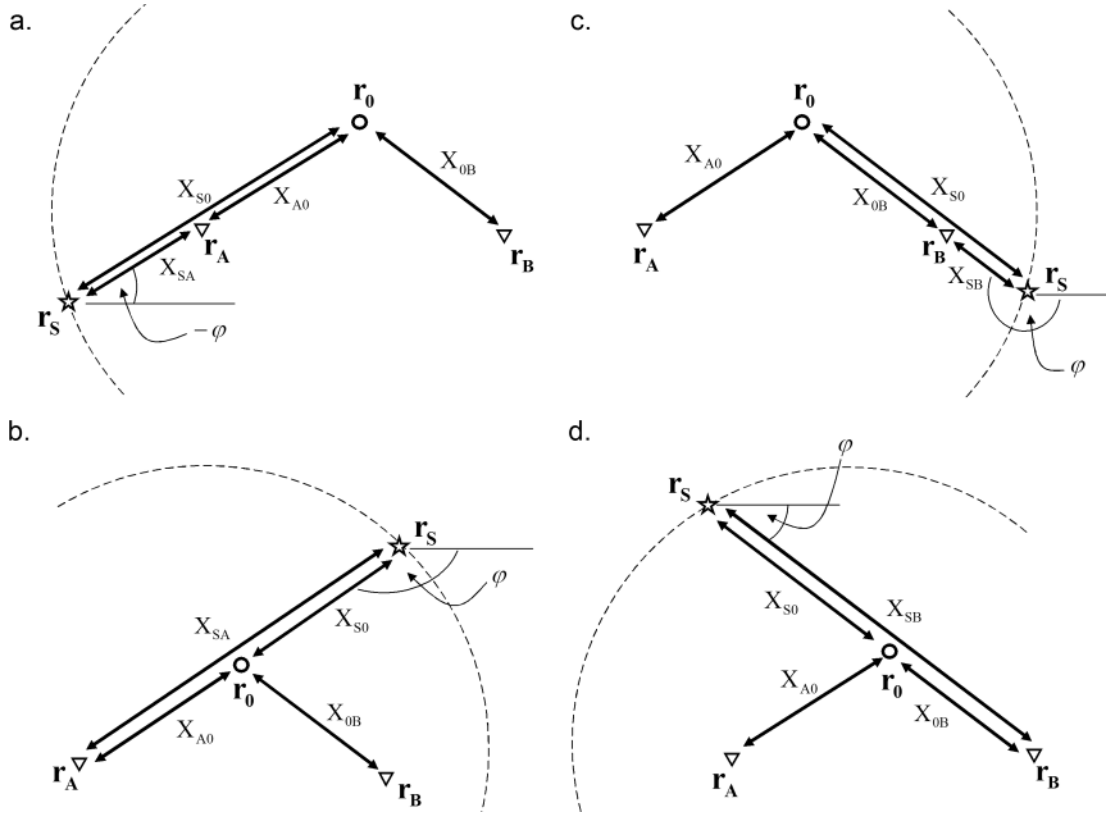

Figure 4. There are four types of stationary point, illustrated by boundary locations, $\mathbf{r}_S$, relating to the recovery of a wave propagating from receiver $\mathbf{r}_A$ to receiver $\mathbf{r}_B$, scattered en route by a heterogeneity at $\mathbf{r}_0$. We use a circular boundary of sources for illustration (dashed line). (a) Term *T2* (physical), (b) Term *T2* (non-physical), (c) Term *T3* (physical) and (d) Term *T3* (non-physical). To illustrate term *T3*, we have defined the additional geometrical term X_{SB}, describing the horizontal offset along the path between the source $\mathbf{r}_S$ and receiver $\mathbf{r}_B$.

waves (and vice versa) and summing the results. The exact scattered surface waves are shown for reference (dashed line). The scattered surface waves have been well estimated, but the non-physical parts of terms *T2* and *T3* can be seen around 1.1–1.3 s lag. As expected, the contribution provided by *T4* (panel c) provides an equal contribution of opposite sign to the non-physical parts of Fig. 6(b); so, after summing all four terms, the correct interreceiver Green's function is recovered (Fig. 6d).

Note that in all of these plots, the lower frequency, earlier arrivals have lower amplitudes in the estimates than in the exact result. Although this error appears to be significant, it is explained by the analysis of Halliday & Curtis (2008), where we derive the necessary frequency-dependent scale factors when sources are present only at the surface of the Earth. We do not apply scaling here, as these errors do not affect the phase of the estimates, neither do they introduce non-physical arrivals.

Although in this example *T4* is small, we later show that it can be large in multiple scattering cases and hence provides a significant contribution to the interferometric integral. In the multiple scattering case, there is more energy in the scattered wavefields between the two receivers, and hence there is more energy in the cross-correlation of the scattered waves (term *T4*). It is also interesting to note that the calculation of terms *T2* and *T3* are equivalent to applications of interferometry where wavefield separation is used. Thus, the non-physical parts of terms *T2* and *T3* are indicative of the types of errors that may be introduced in such applications (e.g. Mehta *et al.* 2007, 2008; Vasconcelos 2007; Vasconcelos & Snieder 2008b).

In Fig. 7, we show the estimate of the full gather of receivers [−16, 0]–[140, 0], from a source at [−140, 0]. Fig. 7(a) shows the directly modelled gather, and Fig. 7(b) shows the interferometric estimate. The amplitude errors can be seen (lower frequencies are stronger in Fig. 7a), but apart from this, both the direct and scattered waves are well recovered. Note that the variation around 180 m offset shows that we have also estimated the radiation pattern of the scatterer. If we had used only point-force sources, this may not have been recovered correctly, as azimuthally dependent scale errors are introduced in that case (e.g. Snieder *et al.* 2006).

2.2 Multiply scattered surface waves

We now illustrate that similar principles apply to multiply scattered surface waves. From the above analysis, we expect the following to occur:

(1) The direct interreceiver surface wave will result from the cross-correlation and summation of the direct source–receiver surface waves recorded at each receiver.

(2) The scattered interreceiver surface waves will result from the cross-correlation of the direct source–receiver surface wave with the scattered source–receiver surface waves (and vice versa).

(3) The cross-correlation of the source–receiver scattered surface waves will account for non-physical arrivals introduced in point 2.

We reproduce the results of the previous section but use a random distribution of 15 scatterers (geometry shown in Fig. 5b). To

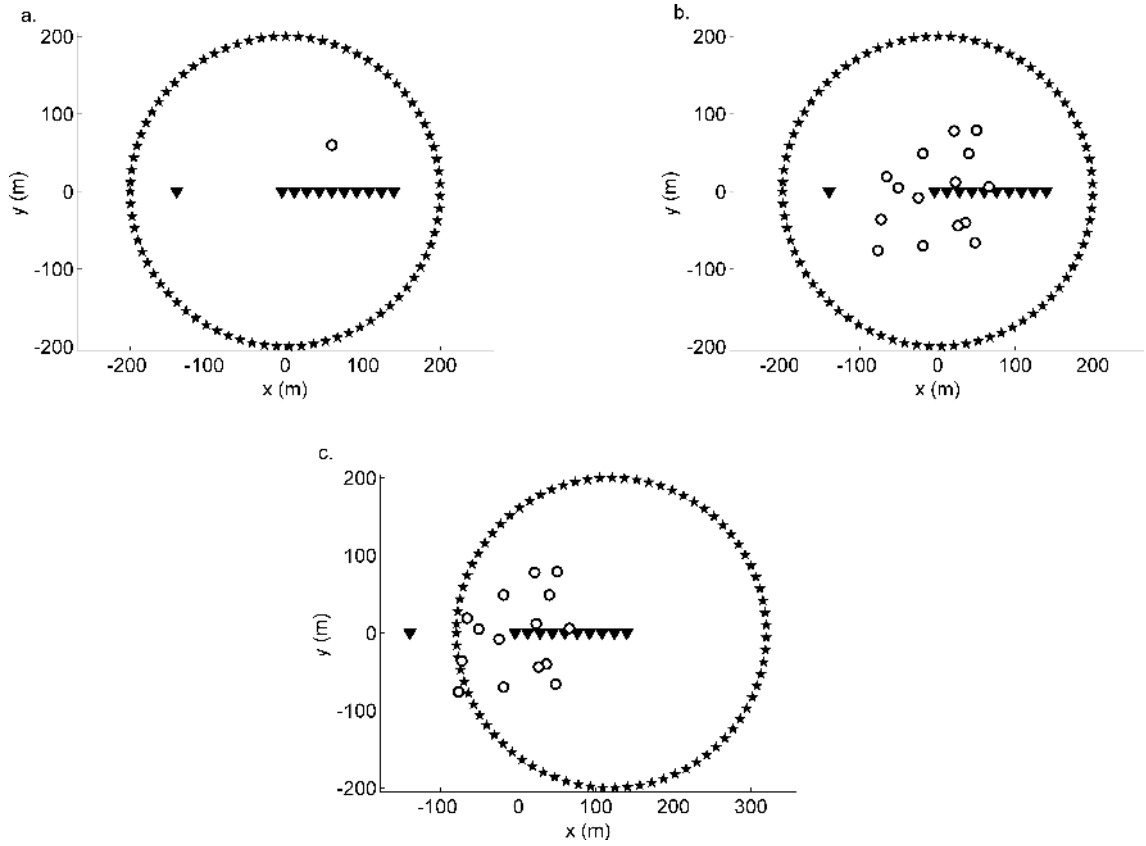

Figure 5. Geometries for testing interferometry for scattered surface waves: (a) single scatterer; (b) multiple scattering and (c) convolution configuration for multiple scattering. Stars indicate source locations, triangles indicate receiver locations, circles indicate point scatterers. Only every fourth source and receiver are plotted for clarity—note that this only applies to the line-array as the left-hand most receiver is isolated.

compute the multiply scattered surface waves, we use a deterministic variant of Foldy's method (Foldy 1945; Groenenboom & Snieder 1995; van Manen *et al.* 2006). This method assumes that there is no angular dependence of the scattering amplitude. Although this assumption is not particularly realistic, it allows us to compute multiply scattered wavefields efficiently within the optical theorem and can still be used to demonstrate the effects discussed herein.

Fig. 8(a) shows the direct waves and is the same as Fig. 6(a). The contribution of the cross-correlation of the direct wave with the scattered waves is shown in Fig. 6(b). This is more complex than that shown in Fig. 6(b), but we observe that the scattered waves are (in parts) well estimated by this step. However, there are many non-physical terms introduced, which we expect to be cancelled by the contribution of term *T4* shown in Fig. 8(c). Fig. 8(d) shows the sum of Figs 8(a)–(c), which results in an approximately correct estimate of the multiply-scattered surface waves. Again, the frequency-dependent amplitude errors are expected, but as described above, these do not affect the phase of the estimate and neither do they introduce spurious arrivals. We show the estimate of the whole gather in Fig. 9, and as expected, both the direct and multiply scattered surface waves are well recovered.

Note that term *T4* has relatively large amplitude (of the same order as the dominant scattered wave). Had we computed the scattered wavefields using a first-order Born analysis (i.e. without the optical theorem), this term would introduce large errors in the interferometric estimates. Hence, when applying interferometry to forward modelled wavefields, the use of the Born approximation is not appropriate to analyse the effects of interferometry on scattered waves. Note that Wapenaar & Fokkema (2006) present a simple single scattering example within the Born approximation, and their interferometric results appear to be exact. This is because, to be consistent with the Born approximation, they include only the zeroth- and first-order terms of the cross-correlations, omitting those terms that would contribute to *T4*.

3 ATTENUATION

In the previous section, we have investigated seismic interferometry for scattered surface waves in a near-ideal setting, using an elastic medium and a well-sampled, closed, 1-D boundary of sources on the ground surface. To achieve exact results would have required a 2-D boundary of sources extending to depth, reducing the similarity between our example and geometrical constraints in practical applications (Wapenaar *et al.* 2004; Snieder *et al.* 2006; Mehta *et al.* 2008). We found that the mutual cancellation of non-physical contributions to the interferometric integral is a key step in producing reliable estimates of the interreceiver surface waves. However, it is unlikely that these near-ideal settings will be achieved in real data applications of the method. Amplitude imbalances (for example, due to attenuation or non-uniform boundary source strength distribution) will result in non-cancellation of these non-physical contributions and the introduction of spurious arrivals. Similar effects will be observed in the case of limited source aperture, where

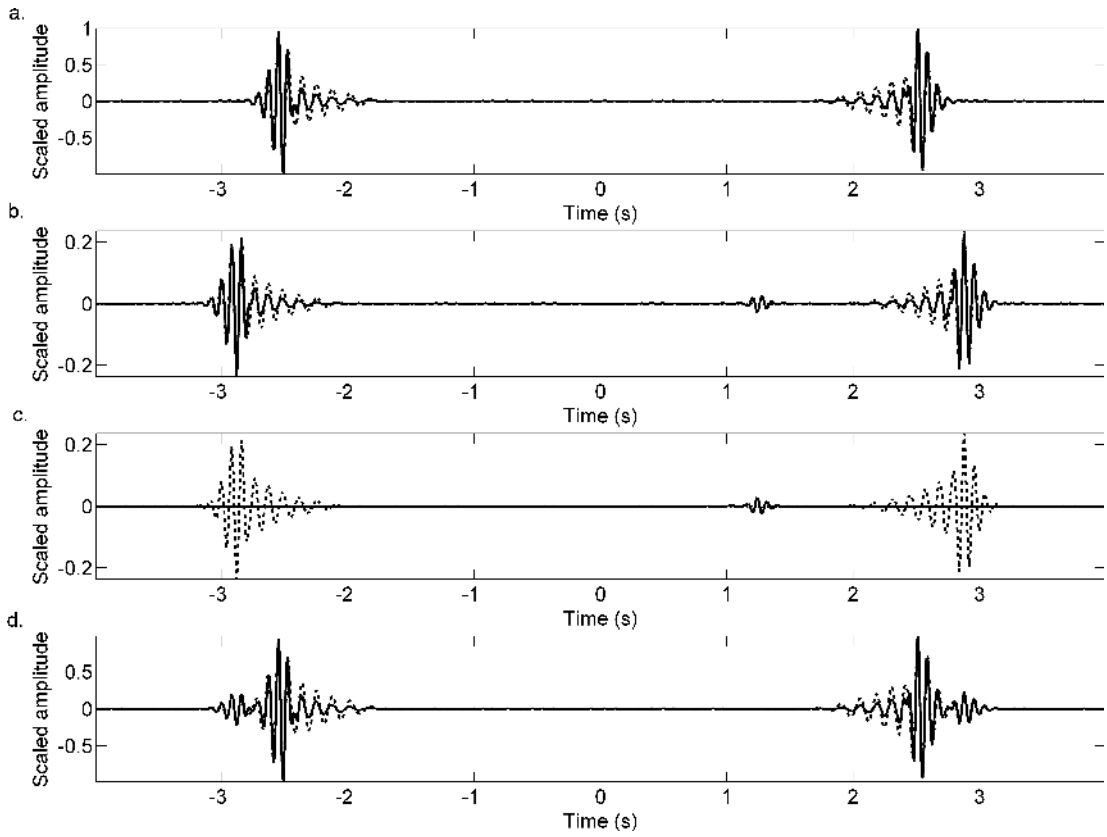

Figure 6. Waveforms for the scattering model in Fig. 5(a). (a) Interferometry using the direct wave only (solid line) and the directly modelled direct wave (dashed line); (b) Interferometry using the direct waves at one receiver and the scattered waves at the other (solid line) and the directly modelled scattered wave (dashed line); (c) Interferometry using the scattered waves only (solid line) and the directly modelled scattered wave (dashed line); (d) Sum of the three contributions above (solid line), with the directly modelled full Green's function for reference (dashed line).

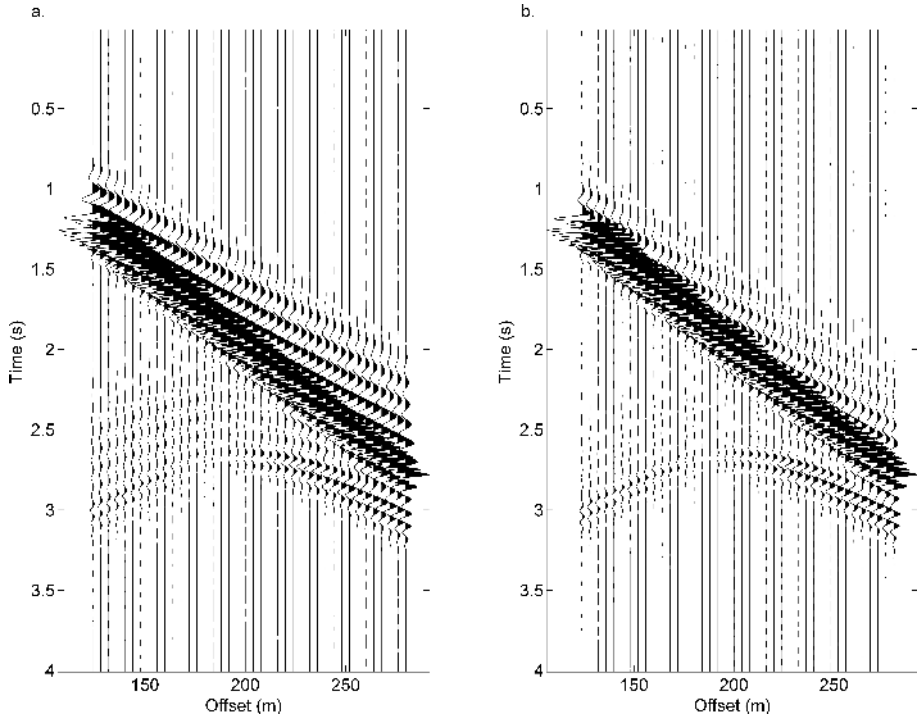

Figure 7. Waveforms for the scattering model in Fig. 5(a). (a) Directly modelled gather for a source at receiver [−140, 0]; (b) Interferometric estimate of the gather in (a). Both plots are for the scattering model in Fig. 5(a). Note that the *x*-axis represents offset, as opposed to the *x*-coordinate plotted in Fig. 5.

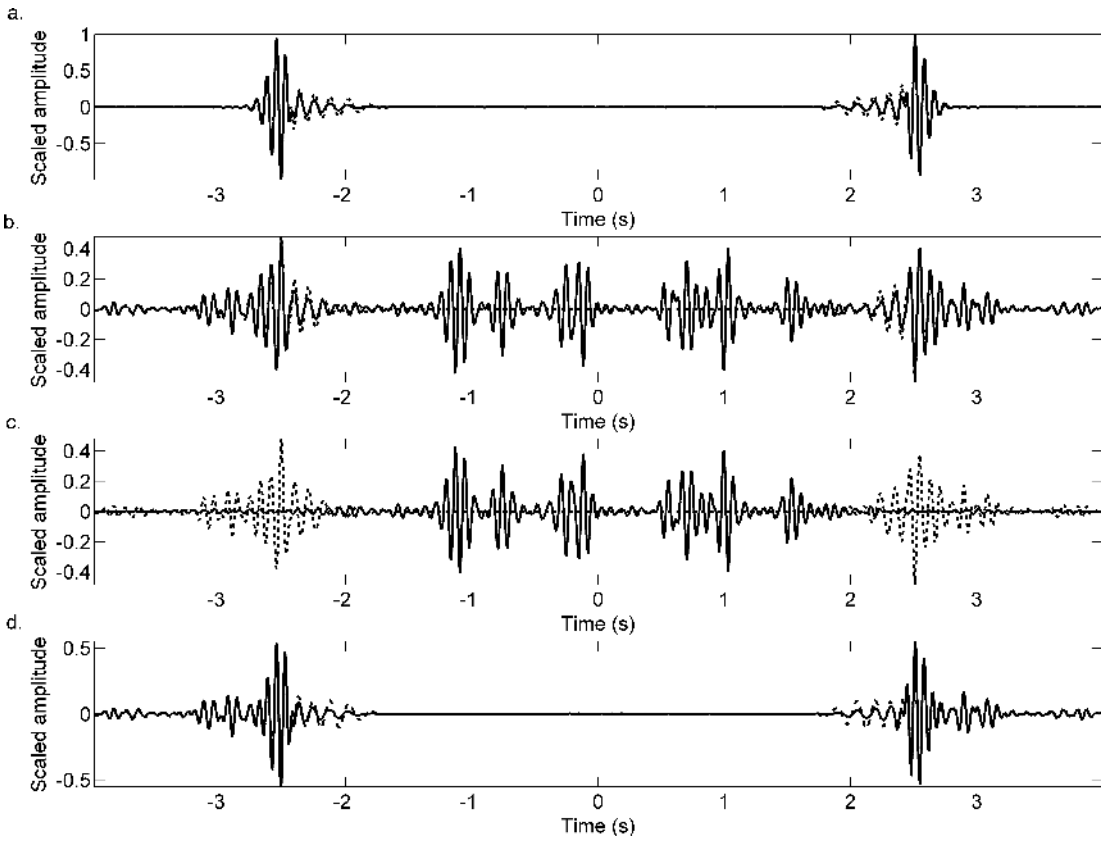

Figure 8. As for Fig. 6, but waveforms are for the scattering model in Fig. 5(b).

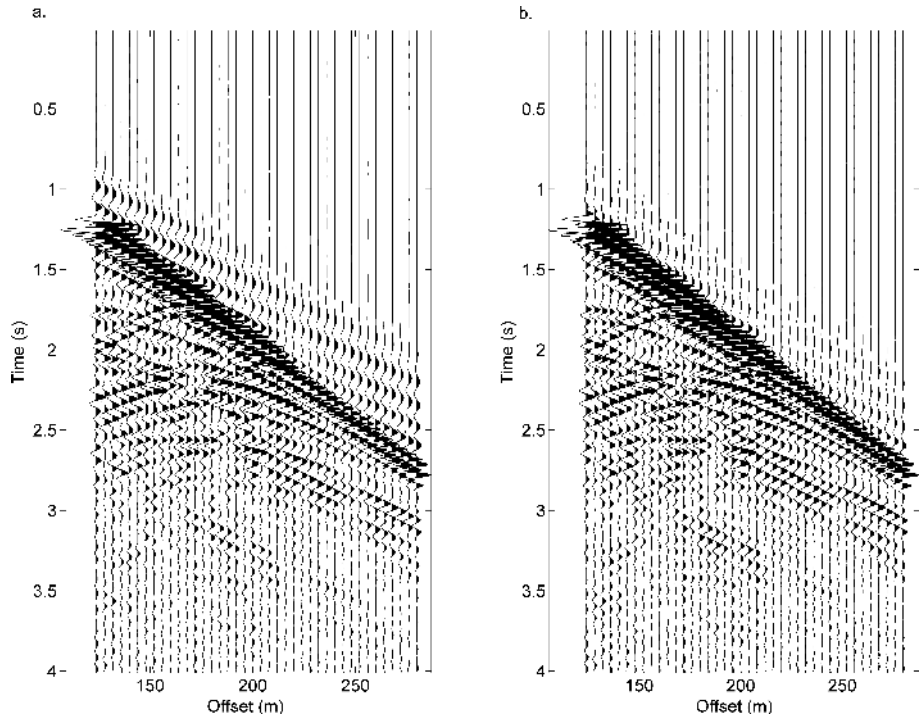

Figure 9. As for Fig. 7, but waveforms are for the scattering model in Fig. 5(b).

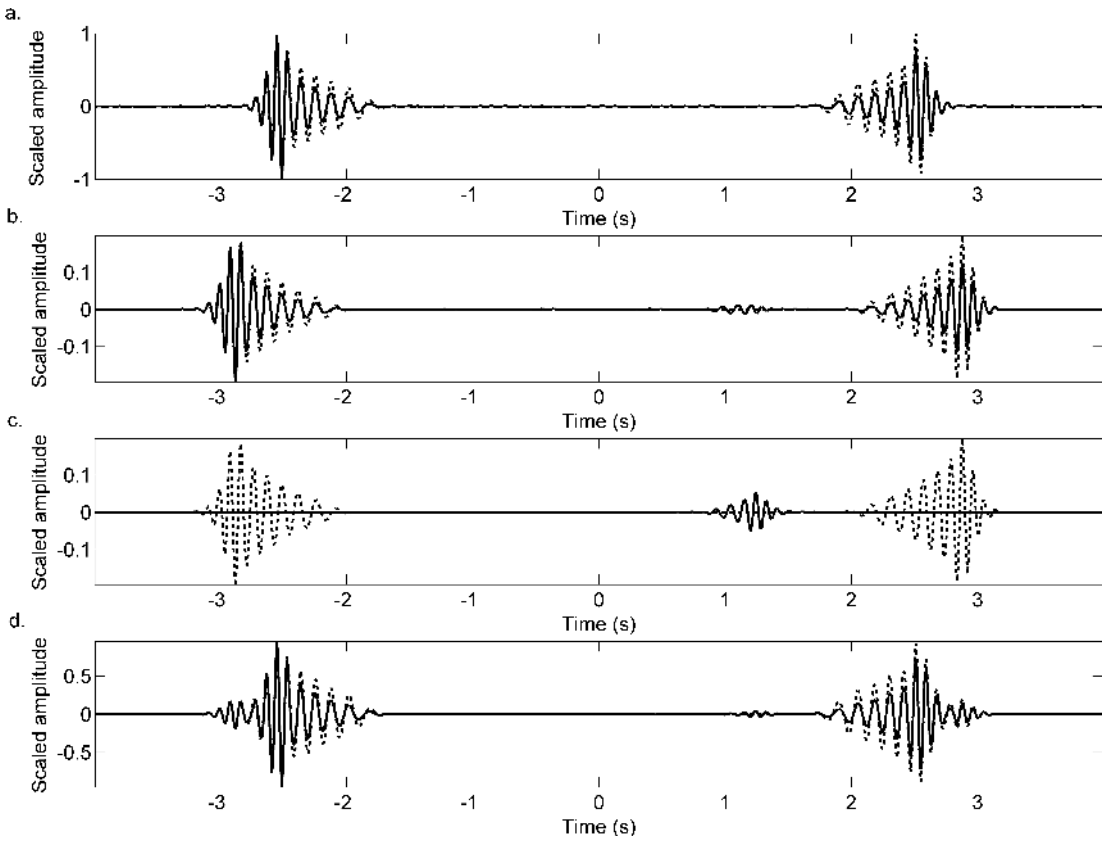

Figure 10. As for Fig. 6, waveforms are for the scattering model in Fig. 5(a), with the introduction of attenuation.

sources may not lie at all of the stationary points required for cancellation.

Cross-correlation based interferometric theory does not account for attenuation, yet the near surface, through which surface waves travel, is often strongly attenuating. We therefore introduce attenuation to illustrate the importance of these cancelling terms. We reproduce our examples using a realistically attenuating medium. To model attenuation, we apply the following offset-dependent damping factor to the calculated surface waves (Aki & Richards 2002, chapter 7.3.4):

$$\exp\left[\frac{(-\omega X)}{2c_v(\omega)Q}\right], \tag{2}$$

where Q is the quality factor (given a value of 50 here), c_v is the phase velocity, ω is the angular frequency and X is the horizontal offset.

Figs 10 and 11 are similar to Figs 6 and 7 showing singly scattered surface waves, but for an attenuating medium. Note that although the scattered surface waves are still recovered, there are changes in amplitude due to the energy lost during propagation between the boundary and each receiver (e.g. compare the causal and acausal parts of Fig. 10a, which would be exactly antisymmetric in the application of eq. 1 to non-attenuating media). Gosselet & Singh (2007) use this symmetry breaking to derive estimates of the quality factor of the medium. This symmetry breaking also has an effect on the parts of terms *T2* and *T3*, which should cancel to give the exact interreceiver surface wave. This un-cancelled term can be seen in the interferometric estimate in both Figs 10(d) (around 1.25 s) and 11(b) (between 1 and 1.5 s for receiver offsets 200–280 m). Fig. 11(b) exhibits time- and offset-dependent amplitude errors due to the presence of attenuation. The amplitude errors are not large here due to the specific geometries used; however, later we show that these errors can indeed be large when less ideal geometries are considered.

For the multiply scattered surface wave case (Figs 12 and 13), the errors are far more abundant due to the complicated nature of the mutually cancelling terms provided by *T2–T4*. This illustrates that the more complex the scattered surface wave field, the larger errors are introduced in the presence of attenuation. The relative amplitudes with respect to both time and offset have not been recovered correctly, but scattered surface waves can still be identified.

Data can be processed to compensate for the effects of attenuation. In exploration seismology, this is often done by applying inverse-Q filters to amplify higher frequencies (e.g. Hargreaves & Calvert 1991; Wang 2002). Application of such methods prior to interferometric processing may allow for enhanced recovery of the higher frequency surface waves, for example, Draganov *et al.* (2008) identify non-physical arrivals in seismic interferometry and estimate a damping factor, which when applied to the data prior to interferometry allows for the elimination of the non-physical arrivals.

There are also adaptations to the interferometric theory that account for the presence of attenuation. For example, Snieder (2007) demonstrates that acoustic wave interferometry can still be applied exactly in the presence of attenuation, provided that energy sources are distributed throughout the medium of propagation, and that the attenuation values are known throughout the medium. A similar formulation could be developed for surface waves, and it may be possible to recover the exact surface waves given a homogeneous distribution of sources at the surface. However, the disadvantage of such an approach is that it requires a model of the medium attenuation.

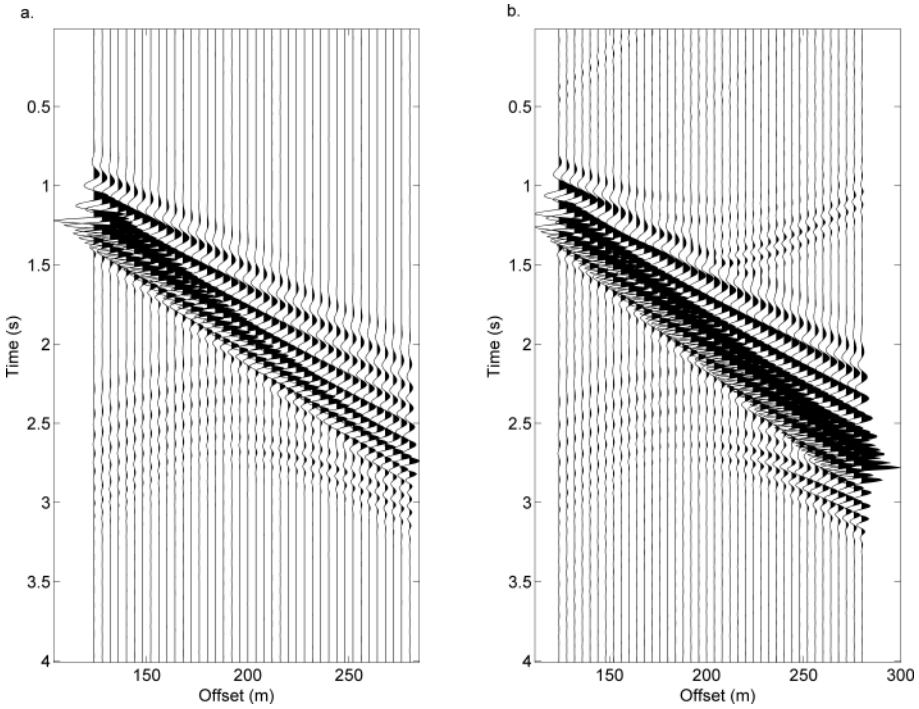

Figure 11. As for Fig. 7, waveforms are for the scattering model in Fig. 5(a), with the introduction of attenuation.

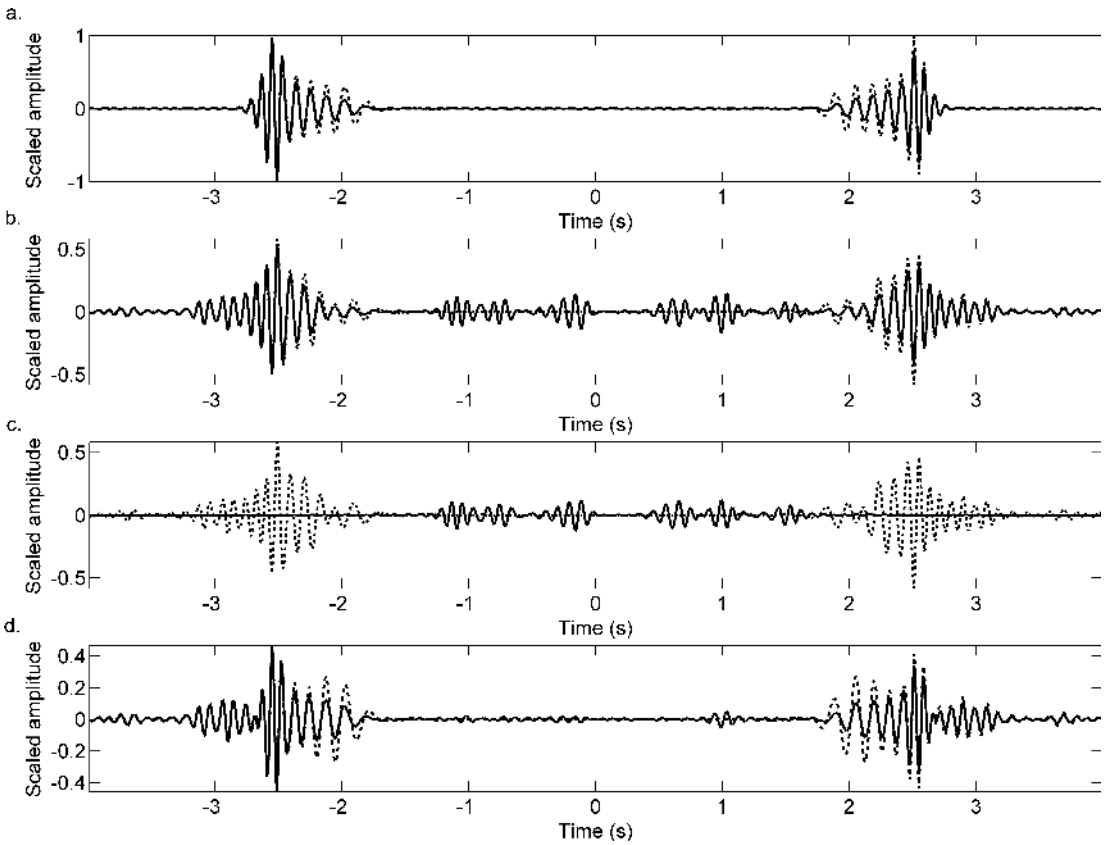

Figure 12. As for Fig. 8, waveforms are for the scattering model in Fig. 5(b) with the introduction of attenuation.

Instead, we concentrate on another approach adapted from the work of Slob *et al.* (2007) and Slob & Wapenaar (2007) in electromagnetic interferometry. Electromagnetic applications often involve very lossy media, and for interferometry to be successfully applied in such media a method to account for wave attenuation must be used. One particularly simple method is to replace cross-correlation with cross-convolution. This is done by deriving interferometric relationships from the reciprocity theorem of the

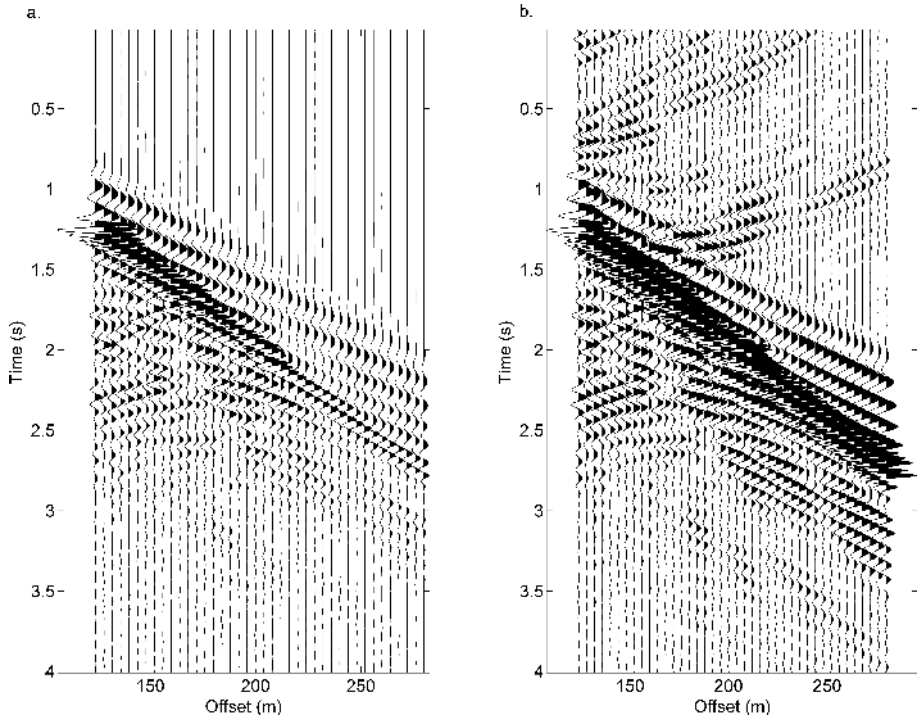

Figure 13. As for Fig. 9, waveforms are for the scattering model in Fig. 5(b) with the introduction of attenuation.

convolution type, as opposed to the reciprocity theorem of the correlation type (e.g. Wapenaar 2007). This new configuration requires that one of the receivers be inside the boundary of sources, whereas the other lies outside of that boundary.

The important difference between correlation- and convolution-type interferometry is that the cross-correlation operator requires time-reversal (or complex conjugation) of one of the inputs whereas the convolution operator does not. Since wavefields cannot be time-reversed in the presence of attenuation, we require that the media be lossless for the application of exact correlation-type interferometry, as expressed by eq. (1). In convolution-type interferometry, we only consider causal Green's functions and no constraints are placed on the attenuation of the medium. In addition, we only recover a causal Green's function, as opposed to the causal and acausal Green's functions recovered using correlation-type interferometry. Hence, we can expect convolution-type interferometry to be useful in the presence of strong attenuation (For a more detailed view on the differences between the correlation- and convolution-type reciprocity theorems, including the presence of volume integrals as considered by Snieder 2007, see de Hoop 1995, e.g. eqs 15.4–7 and 15.5–7).

Rather than simply adapting the findings of Slob *et al.* (2007) and Slob & Wapenaar (2007) for the elastic case, in Appendix B we briefly discuss changes in our stationary-phase analysis of scattered surface waves for the cross-convolution case and find similar results as for the cross-correlation case, term *T1* provides the direct surface wave, and terms *T2* and *T3* combine to provide the scattered surface waves. However, the stationary phase condition for the physical scattered waves changes from $\varphi_{S0} - \varphi_{A0} = 0$ to $\varphi_{S0} - \varphi_{A0} = \pi$, and the stationary phase condition for the non-physical waves changes from $\varphi_{S0} - \varphi_{A0} = \pi$ to $\varphi_{S0} - \varphi_{A0} = 0$. This change is important, as combined with the absence of complex conjugates in convolution-type interferometry, it results in the non-physical arrivals cancelling to zero in the convolution case (see Appendix B). Therefore, no non-physical arrivals are introduced, and term *T4* provides a zero contribution. Thus, we reveal why we expect convolution-type interferometry to perform well in the presence of attenuation or even in cases where the source boundary has limited aperture: since the non-physical arrivals introduced by terms *T2–T4* do not exist in the convolution case, there are no mutually cancelling terms, and there are no errors introduced due to amplitude imbalances or limited aperture, as in the cross-correlation case. Hence, for convolution-type interferometry, the second-order interactions vanish when considering a single-scattering model, and Born-type analysis may be sufficient in this case. Note that this also means that wavefield separation can be applied using convolution-type interferometry, without the introduction of non-physical arrivals—this may be significant if terms *T2* and *T3* are to be calculated using real data to estimate only the scattered wavefield.

To illustrate the convolution case, we use the multiple-scattering model above, shifting the boundary so that receiver [−140, 0] is located externally, with the rest of the receivers located internally; the position of the scatterers relative to the receiver array does not change (Fig. 5c). The corresponding set of results for convolution-type interferometry are shown in Figs 14 and 15; again we expect and observe errors in the lower-frequency, earlier arrivals, as only sources at the surface are used. Compared with Figs 12 and 13, there are no strong errors introduced into the estimates (except for the expected frequency-dependent amplitude errors), and the amplitudes are well recovered. Note that term *T4* provides a small contribution to the estimate; in Appendix B, we show that this is an error in the estimate, as term *T4* should provide a zero contribution. This error occurs due to a pseudo-stationary source point on the surface: Halliday & Curtis (2008) showed that sources at depth are required to correctly construct higher mode surface waves with interferometry, and the current case is similar in nature. The pseudo-stationary source point appears to be stationary when the boundary of sources is confined to the near surface, but in reality, it is not

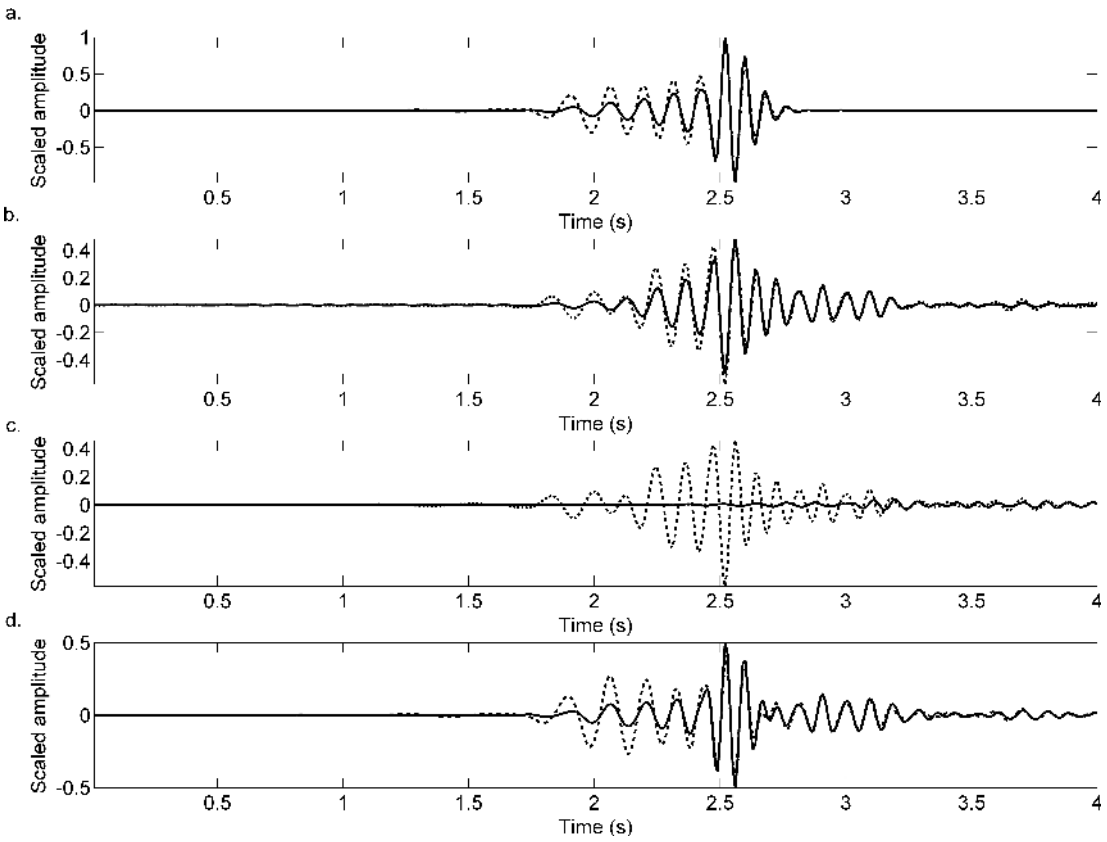

Figure 14. As for Fig. 12, waveforms are for the scattering model in Fig. 5(c), and here we have used convolution-type interferometry in an attenuating medium. Note that convolution-type interferometry does not produce an acausal Green's function, hence only forward times are shown.

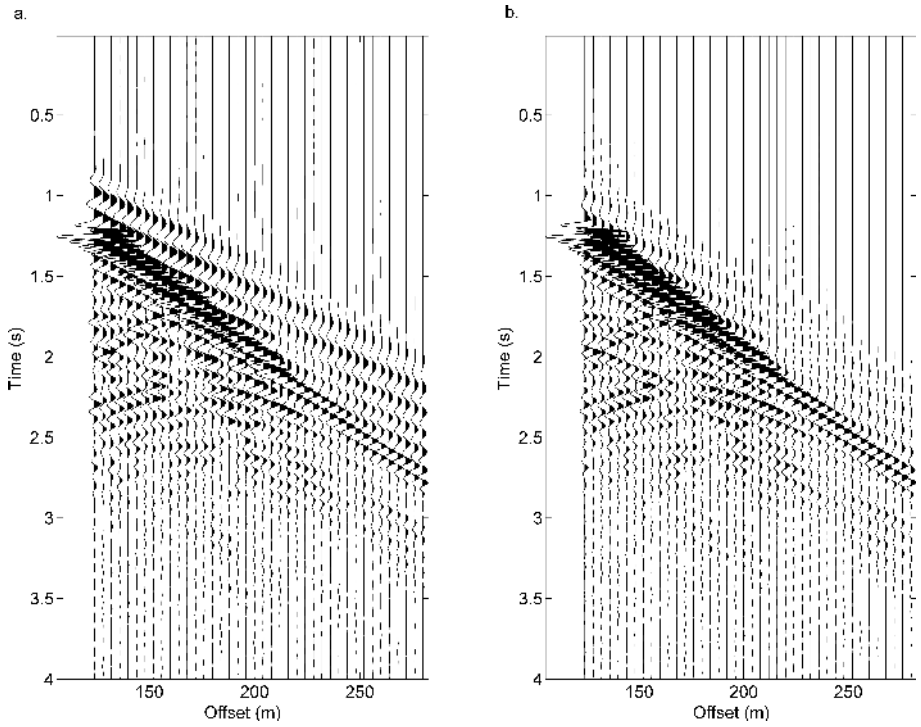

Figure 15. As for Fig. 13, waveforms are for the scattering model in Fig. 5(c), and here we have used convolution-type interferometry in an attenuating medium.

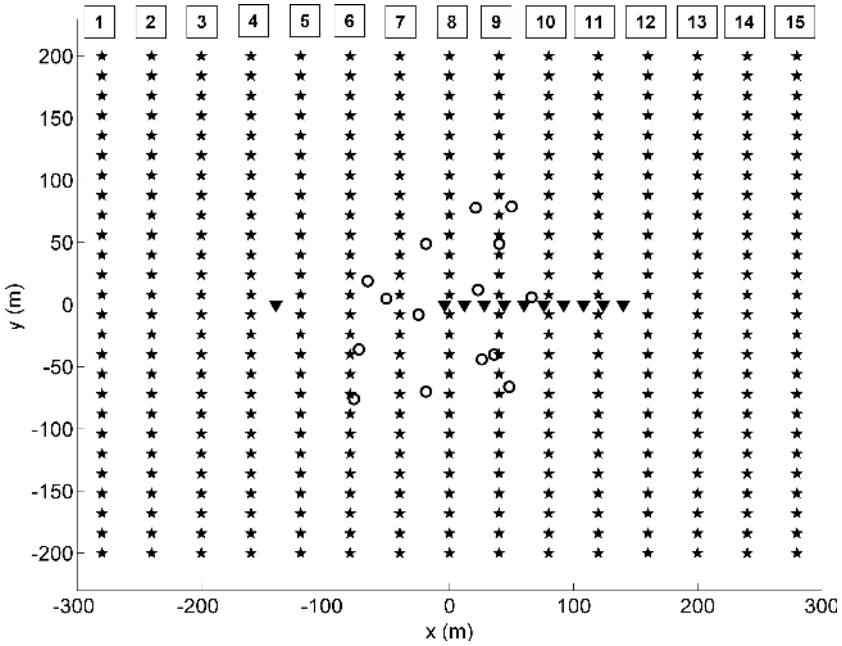

Figure 16. Orthogonal source and receiver geometries used in Figs 17–19. Symbols are as in Fig. 5. Boxed numbers label different source lines.

stationary in the depth direction; so, integration in depth would remove this error. In our example, these errors do not have a strong impact on the resulting surface wave estimates (Fig. 15b). If these errors are large enough to be problematic, then a 'thick' boundary of sources may be used to reduce their effect, as the pseudo-stationary point also varies with surface boundary location (Halliday & Curtis 2008).

4 PRACTICAL SOURCE GEOMETRIES

Up to this point, we have shown that under ideal circumstances, it is possible to make good estimates of interreceiver scattered surface waves using correlation-type interferometry. In attenuating media, correlation-type interferometry introduces errors both in amplitude (in addition to those that we expect due to having only sources at the surface) and in the introduction of spurious arrivals. Convolution-type interferometry does not suffer from the same errors, and the estimates are of higher quality. We now consider some more realistic source distributions in attenuating media ($Q = 50$), using orthogonal source and receiver geometries, typical of exploration surveys on land (Fig. 16). We also consider now the situation where only point-force sources and particle-displacement measurements are available, as typically, these are the only quantities acquired in industrial seismic surveys. Note that rather than using a larger spread of scatterers, we use the same distribution as previously, for ease of comparison with previous results, for computational efficiency of the Foldy modelling method used and because the dominant scatterers are anyway expected to be those located close to the interreceiver line (for example, due to geometrical spreading).

Although these examples demonstrate exploration/engineering-type geometries, the scattering theory presented is not limited to such cases. Accounting for differences in length-scale, frequency and velocity, these geometries could also be considered to represent simplified versions of real life crustal-seismology settings. For example, a line of sources could be illustrative of a coastline, where microseismic energy is released as the waves interact with the coastal shelf, or an active fault plane, where numerous seismic events create a line of sources when considered over long time intervals. A regularly spaced distribution of surface sources might represent the case where background noise is generated in a spatially diffuse manner at the surface, by wind, anthropogenic activity or other near-surface noise sources.

One particular advantage of illustrating our findings using exploration style geometries is that it is easier to observe scattering using linear arrays as opposed to sparsely located receivers. Hence the quality of our interferometric results and the nature of any errors imposed on them, are clearer to the naked eye.

In Fig. 17, we consider the (acausal) contributions from source lines 1–4. Since these receiver lines lie outside of all receiver pairs, we consider correlation-type interferometry. Figs 17(a)–(d) illustrate the contributions from each source line individually, with weighting tapers applied to sources at the end of each line to suppress truncation artefacts (this tapering is applied in all of the following results). Compared with the directly modelled source gather (Fig. 17f), many of the scattering events are well recovered, suggesting that these source lines coincide with stationary points for many of the scattering events. The relative amplitudes are well recovered and the strong errors that were observed prior to the first arrival of the direct surface waves in Fig. 13 are not present here. The relative amplitudes are well estimated here for two reasons: first, the relatively narrow frequency band used (a Ricker wavelet with a central frequency of 15 Hz) means that there are not large differences in attenuation between the lowest ($\sim$10 Hz) and highest ($\sim$20 Hz) peak frequencies. Second, the distance between one source line and the closest receiver for each pair in the gather is always constant, that is, the nearest receiver to the source line is always the same. Hence, at least for the direct surface wave, the energy lost due to attenuation before the first receiver is encountered is the same for each receiver pair. This is not true for the scattered waves, and we expect energy loss to vary accordingly.

Fig. 17(e) shows the sum of all four estimated gathers (after normalization of each gather to a maximum amplitude of one to account for varying amplitudes in the estimates from different source lines, ensuring that each provides an equal contribution to the sum).

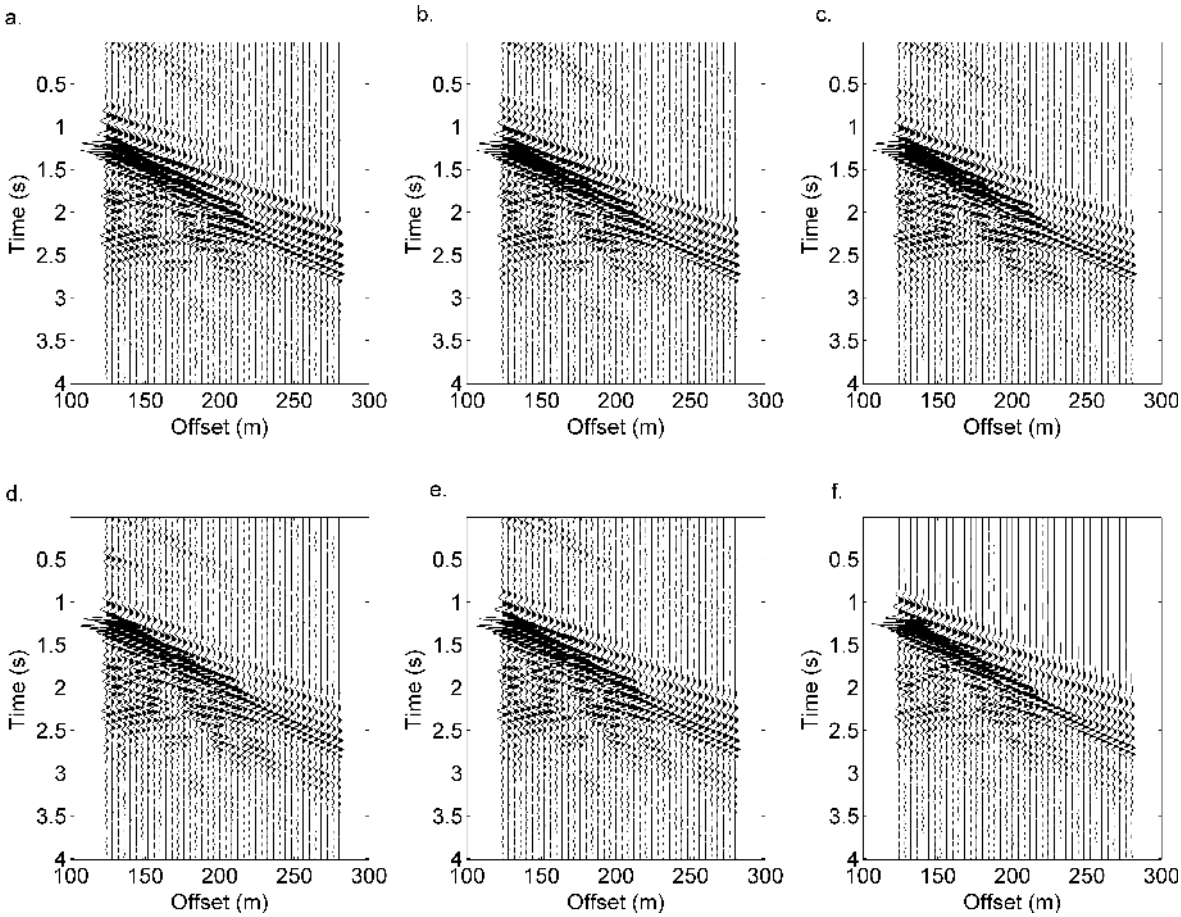

Figure 17. (a)–(d) Correlation-type interferometric estimates in the presence of attenuation of a gather at source location [0, −140], using source lines from 1 to 4 individually; (e) Sum of panels (a)–(d) after normalization of each gather to maximum amplitude of one; (f) Directly modelled source gather.

Some of the errors (e.g. the event observed to moveout from 0s at 124 m offset) do not vary with source line position and hence sum constructively. This is expected from our stationary-phase analysis of a scattering medium, as the phase of these errors (introduced by non-cancellation of the non-physical parts of *T2* and *T3* and the whole of *T4*) is stationary for any boundary source configuration. This is different from other errors in interferometry for cross-mode contributions identified previously by Halliday & Curtis (2008) or from the ghost events identified by Draganov *et al.* (2004), both of which diminish when neighbouring source boundaries are used and the results stacked.

In Fig. 18, we take source lines 12–15 and repeat the estimation process used in Fig. 17. Fig. 18(a)–(d) again illustrate the (causal) estimates using each source line. These results differ greatly from those in Fig. 17. First, the relative amplitudes with respect to time and offset are incorrect compared with the directly modelled results in Fig. 18(f). This is because, for these geometries, the distance from a source line to the nearest receiver is not constant for each pair in the receiver array, that is, the position of the nearest receiver relative to the source line varies for each pair. Hence there are different source–receiver energy losses for each receiver pair, producing erroneous relative amplitudes, and due to these losses, the energy travelling between the virtual source and each receiver is less than in the case illustrated in Fig. 17. The weaker direct surface waves may amplify the appearance of the non-physical arrivals discussed below. Second, many of the scattered surface wave arrivals are not constructed, most notably those around 124–200 m offset. This is because, for this particular geometry and distribution of scatterers, the source lines miss a lot of the stationary points for the scattered surface waves. However, as can be seen by the strong events prior to the arrival of the direct surface wave, these source lines include stationary points for the non-physical part of the integral (i.e. the non-physical parts of *T2* and *T3* identified above and in eqs A28 and A30 of Appendix A). Finally, here we can see that the strong spurious arrivals have the same phase across all four estimates and again stack constructively in Fig. 18(e). These two sets of results (Figs 17 and 18) illustrate the sensitivity of the cross-correlation approach to non-physical arrivals introduced by attenuation and limited aperture. These two cases represent extreme situations: in Fig. 17, results seem favourable, but by considering the same scattering and receiver geometry with a different source distribution, the results deteriorate greatly.

In Fig. 19, we use source lines 5–7 in Fig. 16. Each of these source lines lies between the receiver at [−140, 0] and all other receivers. We therefore use convolution-type interferometry in this case. Fig. 19(a)–(c) show the estimates from each source line. The scattered surface waves are well estimated from all gathers. Note that there are no strong spurious arrivals prior to the arrival of the direct surface wave, but we do observe amplitude anomalies. For example, there is a relatively strong event in the interferometric estimates moving out from 2.6 s at 124 m offset to 3.2 s at 200 m offset, which is present, but much weaker, in Fig. 19(e).

Slob *et al.* (2007) identified that spurious arrivals in convolution-type interferometry are different from those observed in correlation-type interferometry and propose the combination of the two methods

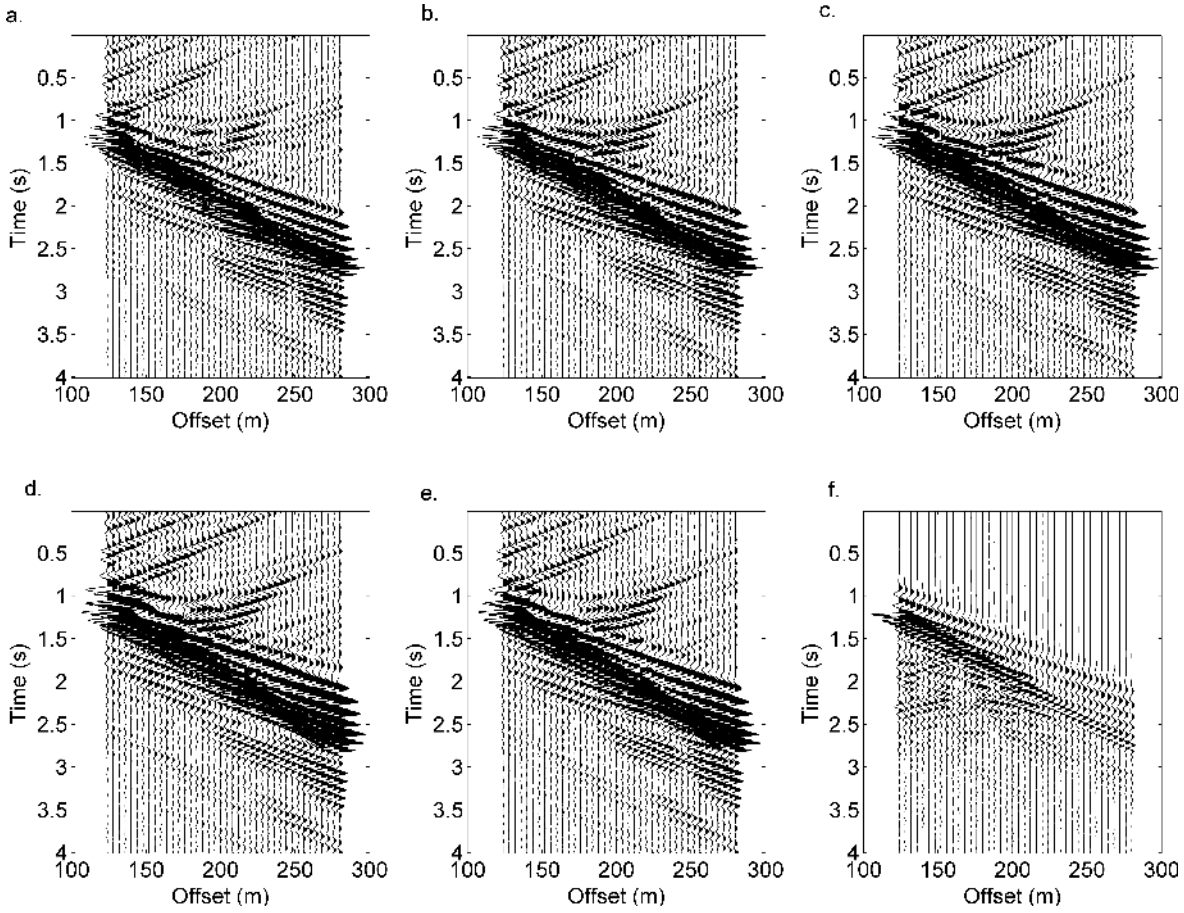

Figure 18. (a)–(d) Correlation-type interferometric estimates in the presence of attenuation of a gather at source location [0, −140] using the four right-hand most source lines; (e) Sum of panels (a)–(d) after normalization of each gather; (f) Directly modelled source gather.

to identify which arrivals are physical and which are non-physical. However, it remains unclear as to how this can be achieved, other than by comparison to find those events constructed by both methods. We must be careful, however, as this approach may not be suitable for scattered surface waves. For example, if we were to compare the results in Fig. 19 with those in Figs 17 and 18 individually, the comparisons would vary significantly. Figs 17 and 19 compare favourably and both contain many of the same scattered events. However, comparing Fig. 19 with Fig. 18, many scattering events are not estimated in the latter; so, it is difficult to identify which (if any) of the scattering events recovered in Fig. 19 are spurious. Note that in the exploration case, it is possible that estimates can be checked against the actual source–receiver data, from which we may wish to remove the surface waves.

The results shown here indicate that it is possible to make estimates of scattered surface waves in attenuating media using realistic source geometries and using only point-force sources. The cross-correlation results indicate that the quality of the estimate varies depending on the geometries of the chosen sources and receivers—in our examples, certain source geometries are affected more by attenuation and certain source geometries also miss stationary points for scattered surface waves. By also producing results for convolution-type interferometry, we obtain an additional set of estimates. By applying the convolution-type approach to our example, we observe the relative insensitivity of the method to non-physical arrivals, which may be introduced due to the effects of attenuation and limited aperture. This is explained by our stationary-phase analysis, which indicates that there are only physical contributions to interferometry in the convolution-type approach, whereas in the correlation-type approach, there are non-physical events, which may not cancel in non-ideal circumstances.

5 DISCUSSION

In correlation-type seismic interferometry for scattered surface waves, the presence of attenuation introduces time- and offset-dependent amplitude errors and strong spurious arrivals. The latter relate to non-cancellation of contributions from stationary points that would cancel if there were no energy losses. Since these cancelling contributions are second order in the sense of being an interaction of two scattered fields, first-order (Born) theory does not provide correct analysis of correlation-type interferometry, even for singly-scattered waves.

Vasconcelos (2007) derives an expression to account for these cancelling terms when interferometry is applied using wavefield separation. This requires a volume integral that accounts for energy losses due to backscattering from heterogeneities along paths between boundary-source positions and receiver locations. Snieder (2007) derives a similar expression to account for energy losses along stationary paths due to anelastic attenuation. These expressions are

$$\mathrm{i}\omega \int_{r\in V} (\kappa_0 - \kappa) G_0(\mathbf{r}, \mathbf{r}_\mathrm{A}) G^*(\mathbf{r}, \mathbf{r}_\mathrm{B}) \mathrm{d}V \qquad (3)$$

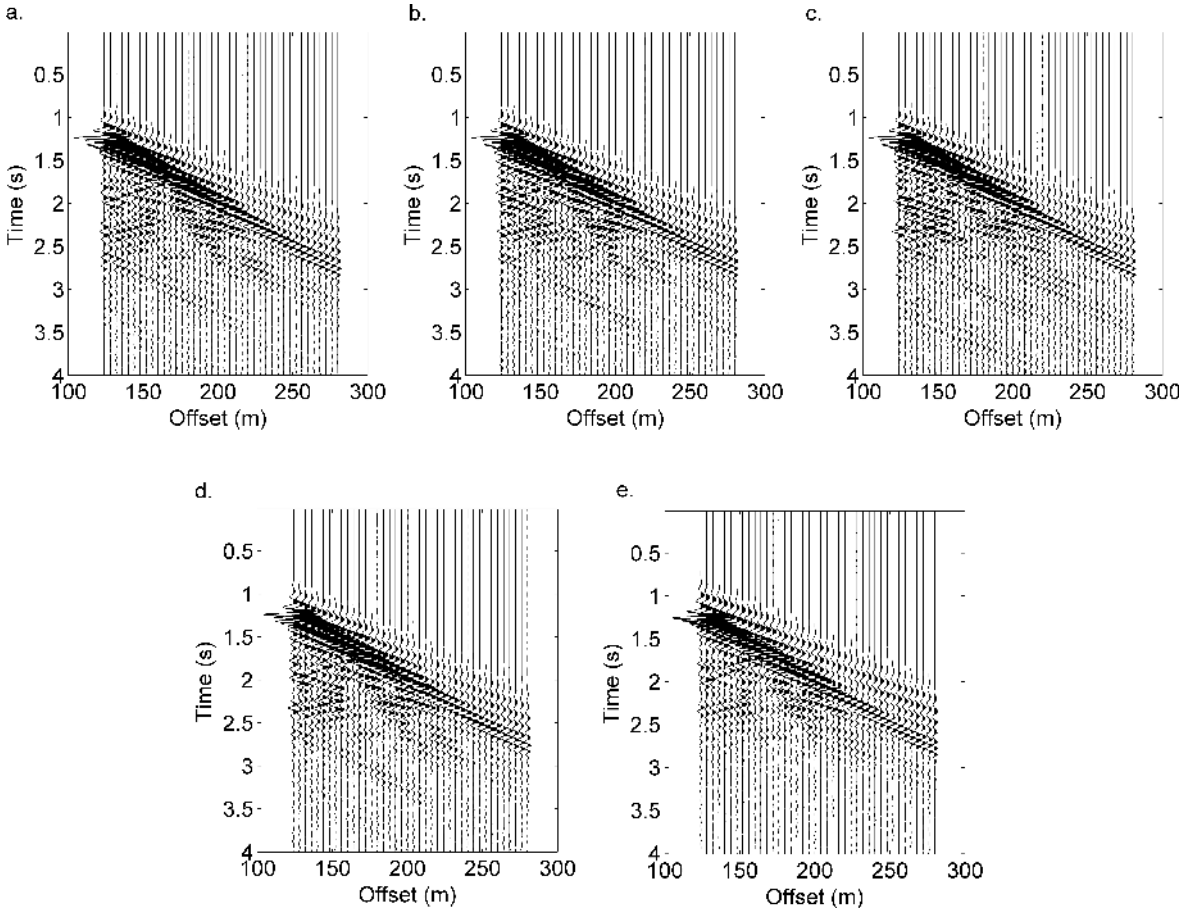

Figure 19. (a)–(c) Estimates using convolution-type interferometry in the presence of attenuation of a gather at source location [0, −140] using source lines 5, 6 and 7 in Fig. 16; (d) Sum of panels (a)–(c) after normalization of each gather; (e) Directly modelled source gather.

and

$$2\omega \int_{r\in V} \kappa_{\mathrm{i}} G(\mathbf{r}, \mathbf{r}_{\mathrm{A}}) G^{*}(\mathbf{r}, \mathbf{r}_{\mathrm{B}}) \mathrm{d}V \tag{4}$$

respectively, where G_0 is the Green's function in the background medium, G is the full Green's function, $(\kappa_0 - \kappa)$ is the medium (compressibility) perturbation and κ_{i} is the imaginary part of the compressibility. In the analysis of Vasconcelos (2007), $\kappa_{\mathrm{i}} = 0$, and integrals such as Snieder's would vanish. However, the similarity of these expressions suggests that the two effects are not unrelated; we can expect that volume integration over both the medium perturbations and the anelastic properties of the medium will be required to account for these non-cancelling terms in the presence of attenuation. Indeed, we noted in Section 3 that the errors due to un-cancelled non-physical events in the presence of attenuation are more abundant when the medium has greater complexity.

These spurious arrivals do not appear when we consider convolution-type interferometry; since there are no mutually cancelling terms, spurious arrivals are not introduced due to attenuation. Therefore, where appropriate geometries are available, we propose that the convolution-type approach be used in place of (or in addition to) correlation-type interferometry (convolution-type interferometry requires the boundary of sources to intersect the interreceiver path). What is more, for singly scattered waves, Born theory is correct for convolution-type interferometry.

Using more practical source geometries, we have illustrated the difference in errors introduced between the convolution case and the cross-correlation case. A combined approach may therefore help identify spurious arrivals and select the best available estimates of the scattered surface waves as proposed previously for electromagnetic applications (Slob *et al.* 2007; Slob & Wapenaar 2007). Although this may be appropriate in electromagnetic applications, we have illustrated that it may not be suitable when considering scattered surface waves, as with restricted source geometries, some scattering events may not appear in the interferometric estimate for one type of interferometry, but they may for the other. It then becomes difficult to discriminate between real scattered events and those that are spurious or non-physical. In exploration applications, in which surface waves are to be removed from source–receiver data, this is less of a problem due to the presence of the actual source–receiver data, which can act as an extra control, against which to check the estimates.

In natural- or passive-source seismology, we can only use sources that nature makes available. However, we know a lot about such sources. Extensive earthquake catalogues exist, and specific events can be selected to create a chosen boundary of sources (provided those earthquakes have been observed at all receivers of interest). The growing interest in seismic interferometry has created a better understanding of the sources of ambient noise, which are used in passive interferometry (e.g. Stehly *et al.* 2006; Pedersen *et al.* 2007), and further to this, new methods, such as time-reversed focusing, can be used to identify sources of ambient noise (Rhie & Romanowicz 2004, 2006; Steiner *et al.* 2008). With this in mind, it should be possible to identify locations (1) where we expect to

observe interreceiver scattered surface waves and (2) where sources that may allow us to recover these using seismic interferometry are available (e.g. by forming orthogonal source lines or closed boundaries of sources at the surface of the Earth, which will cover stationary points for scattered surface waves). To date, the vast majority of applications of seismic interferometry in such settings utilize the correlation-type integral. However, our findings suggest that better results may be obtained using the convolution-type integral, and for surface waves, it can be relatively straightforward to find appropriate geometries of sources and receivers.

If scattered surface waves can be recovered successfully, it may be possible to apply more complex inversion methods in passive seismic tomography. Methods accounting for scattered surface waves, such as those of Snieder (1986, 2002), Snieder & Nolet (1987), Meier *et al.* (1997), Marquering *et al.* (1999), Spetzler *et al.* (2002) and Ritzwoller *et al.* (2002), can take into account heterogeneities that lie off the great circle path and do not rely on the assumption that heterogeneities are of the same scale as the Fresnel zone or the dominant wavelength (as used in ray geometrical tomography). This would allow the capabilities of seismic interferometry to be extended, allowing for more detailed imaging of the Earth's subsurface.

In exploration seismology, the successful recovery of scattered surface waves would allow for the adaptive removal of those surface waves from seismic surveys. Cross-line scattered surface waves are a particularly difficult form of noise to remove, and subsurface image quality is often compromized in areas with strong scattering. Interferometry provides an alternative method by which these arrivals can be estimated and then subtracted from source–receiver data, without the need for single scattering approximations and inverse scattering schemes (e.g. such as in Blonk *et al.* 1995; Blonk & Herman 1996; Ernst *et al.* 2002a,b; Campman *et al.* 2005; Campman *et al.* 2006; Herman & Perkins 2006) or the use of arrays required for acquisition-based methods (e.g. such as in Morse & Hildebrandt 1989; Regone 1998; Özbek 2000a,b).

Although we have focused on correlation- and convolution-type interferometry, recent advances have illustrated that deconvolution is a valuable tool in seismic interferometry and may also be suitable for application in attenuative media (Vasconcelos & Snieder 2008a,b; Wapenaar *et al.* 2008).

6 CONCLUSIONS

A stationary phase analysis of the interferometric integral for scattered surface waves has been used to illustrate the contributions involved in correctly recovering the interreceiver scattered surface wave, complimenting our previous work on the recovery of interreceiver direct multimode surface waves (Halliday & Curtis 2008). This analysis reveals key differences between the stationary-phase analysis of seismic interferometry for reflected and scattered wavefields.

This analysis is illustrated using synthetic scattered surface waves. We considered both single- and multiple-scattering models and confirmed the following observations from our theoretical analysis:

(1) The direct surface wave is recovered from the cross-correlation of the direct surface waves only—previously shown by Snieder (2004b) and by Halliday & Curtis (2008).

(2) The interreceiver scattered surface wave is recovered from the cross-correlation of the direct surface waves with the scattered surface waves. This set of cross-correlations also introduces a spurious or non-physical arrival.

(3) When scattering amplitudes are determined within the optical theorem, the spurious arrival introduced in step 2 is cancelled by the cross-correlation of the scattered surface waves observed at both receivers.

To solve for the correct scattered surface waves using the stationary phase analysis, we observe that scattering amplitudes must have complex values, with the constraints on these values governed by the optical theorem for surface waves. Here we treat the particular case of isotropic density perturbations and derive the constraints that the optical theorem places on the scattering amplitude. This emphasizes the importance of the optical theorem in such cases and of stationary phase analysis in furthering the understanding of physical phenomena.

The addition of attenuation into our examples causes further problems. Errors in amplitude due to energy losses result in steps 2 and 3 above not providing mutually cancelling terms. The direct and scattered surface waves can still be seen, but they exhibit amplitude errors. We have shown that by using convolution-type interferometry, it is possible to avoid these errors, as this variation of the method accounts for attenuating media and is less sensitive to the non-physical arrivals introduced by limited aperture.

We also find that a first-order Born analysis is not suitable for analysing the effects of correlation-type interferometry on scattered wavefields, although due to the absence of the non-physical parts of terms *T2* and *T3*, such a Born analysis suffices when considering convolution-type interferometry.

We then consider more realistic geometries, representative of a 3-D seismic survey but also, perhaps, of other passive situations, such as a coastline emitting microseisms, an active fault plane or distributed anthropogenic noise sources. These illustrate that different geometries are affected differently by attenuation, and certain geometries also result in the omission of stationary points for scattered surface waves. The use of convolution-type interferometry provides estimates that exhibit different types of errors from those seen in correlation-type interferometry. It may be possible to combine the two methods to identify those events that are errors and those that are real events (as proposed for the electromagnetic case). One might then select the source geometries that result in the best estimates.

Seismic interferometry has great potential. Successful recovery of more detailed seismograms, including features such as scattered surface waves, may go some way to seeing this potential realized. In exploration geophysics, this can allow for removal of scattered surface waves, allowing for more reliable subsurface imaging. In near-surface geophysics, scattered surface waves can be used to invert for near-surface properties, and in regional and global seismology, this can allow for the application of more complex tomography and imaging schemes, allowing the additional information contained in scattered waves to be put to use to create more informative images of the Earth's crust and upper mantle.

ACKNOWLEDGMENTS

We would like to thank Deyan Draganov, Kasper van Wijk and Roel Snieder for their encouraging reviews and valuable comments. We acknowledge the support from the Scottish Funding Council for the Joint Research Institute with the Heriot-Watt University which is

a part of the Edinburgh Research Partnership in Engineering and Mathematics (ERPem).

REFERENCES

Aki, K. & Richards, P.G., 2002. *Quantitative Seismology,* University Science Books, CA.

Bakulin, A. & Calvert, R., 2004. Virtual Source: new method for imaging and 4D below complex overburden, in *Proceedings of the 74th Annual International Meeting, SEG,* Expanded Abstracts, pp. 2477–2480.

Bakulin, A. & Calvert, R., 2006. The virtual source method: theory and case study, *Geophysics,* **71,** SI139–SI150.

Blonk, B. & Herman, G.C., 1996. Removal of scattered surface waves using multicomponent seismic data, *Geophysics,* **61,** 1483–1488.

Blonk, B., Herman, G.C. & Drijkoningen, G.G., 1995. An elastodynamic inverse scattering method for removing scattered surface waves from field data, *Geophysics,* **60,** 1897–1905.

Brandenburg, A. & Snieder, R., 1989. The attenuation of surface waves due to scattering, *Geophys. J.,* **8,** 183–194.

Campillo, M. & Paul, A., 2003. Long-range correlations in the diffuse seismic coda, *Science* **299,** 547–549.

Campman, X.H. & Riyanti, C.D., 2007. Non-linear inversion of scattered seismic surface waves, *Geophys. J. Int.,* **171,** 1118–1125.

Campman, X.H., van Wijk, K., Scales, J.A. & Herman, G.C., 2005. Imaging and suppressing near-receiver scattered surface waves, *Geophysics,* **70,** V21–V29.

Campman, X.H., Herman, G.C. & Muyzert, E., 2006. Suppressing near-receiver scattered waves from seismic land data, *Geophysics,* **71**.

Claerbout, J.F., 1968. Synthesis of a layered medium from its acoustic transmission response, *Geophysics,* **33,** 264–269.

Curtis, A., Gerstoft, P., Sato, H., Snieder, R. & Wapenaar, K., 2006. Seismic interferometry—turning noise into signal, *Leading Edge,* **25,** 1082–1092.

de Hoop, A.T., 1995. *Handbook of Radiation and Scattering of Waves,* Academic Press, San Diego.

Dong, S., He, R. & Schuster, G., 2006. Interferometric prediction and least squares subtraction of surface waves, in *Proceedings of the 76th Annual International Meeting, SEG,* Expanded Abstracts, pp. 2783–2786.

Draganov, D., Wapenaar, K. & Thorbecke, J., 2004. Passive seismic imaging in the presence of white noise sources, *Leading Edge,* **23,** 889–892.

Draganov, D., Ghose, R., Ruigrok, E., Thorbecke, J. & Wapenaar, K., 2008. Effect of intrinsic losses on seismic interferometry, in *Proceedings of the 70th EAGE Conference and Exhibtion,* Rome.

Ernst, F., Herman, G.C. & Blonk, B., 2002a. Reduction of near-surface scattering effects in seismic data, *Leading Edge,* **17,** 759.

Ernst, F., Herman, G.C. & Ditzel, A., 2002b. Removal of scattered guided waves from seismic data, *Geophysics,* **67,** 1240–1248.

Foldy, L.L., 1945. The multiple scattering of waves; I: general theory of isotropic scattering by randomly distributed scatterers, *Phys. Rev.,* **67,** 107–119.

Gertstoft, P., Sabra, K.G., Roux, P., Kuperman, W.A. & Fehler, M.C., 2006. Green's functions extraction and surface-wave tomography from microseisms in southern California, *Geophysics,* **71,** SI23–SI31.

Gosselet, A. & Singh, S.C., 2007. Using symmetry breaking in time-reversal mirror for attenuation determination, *SEG Exp. Abs.,* **26,** 1639–1643.

Groenenboom, J. & Snieder, R., 1995. Attenuation, dispersion and anisotropy by multiple scattering of transmitted waves through distributions of scatterers, *J. acoust. Soc. Am.,* **98,** 3482–3492.

Halliday, D.F. & Curtis, A., 2008. Seismic interferometry, surface waves, and source distribution, *Geophys. J. Int.,* **175,** 1067–1087.

Halliday, D.F. & Curtis, A., 2009. A generalized optical theorem for surface waves and layered media, *Phys. Rev. E.,* in press.

Halliday, D.F., Curtis, A. & Kragh, E., 2008. Seismic surface waves in a suburban environment—active and passive interferometric methods, *Leading Edge,* **27,** 210–218.

Hargreaves, N.D. & Calvert, A.J., 1991. Inverse-*Q* filtering by Fourier transform, *Geophysics,* **56,** 519–527.

Herman, G.C. & Perkins, C., 2006. Predictive removal of scattered noise, *Geophysics,* **71,** V41-V49.

Herman, G.C., Milligan, P.A., Huggins, R.J. & Rector, J.W., 2000. Imaging shallow objects and heterogeneities with scattered guided waves, *Geophysics,* **65,** 247–252.

Kaslilar, A., 2007. Inverse scattering of surface waves: imaging of near-surface heterogeneities, *Geophys. J. Int.,* **171,** 352–367.

Levander, A., 1990. Seismic scattering near the earth's surface, *Pure appl. Geophys,* **132**.

Lobkis, O.I. & Weaver, R.L., 2001. Ultrasonics without a source: thermal fluctuation correlations at MHz frequencies, *Phys. Rev. Lett.,* **87**.

Malcolm, A.E., Scales, J.A. & van Tiggelen, B.A., 2004. Extracting the Green function from diffuse, equipartitioned waves, *Phys. Rev. E,* **70,** 015601

Marquering, H., Dahlen, F.A. & Nolet, G., 1999. Three-dimensional sensitivity kernels for finite-frequency traveltimes: the banana-doughnut paradox, *Geophys. J. Int.,* **137,** 805–815.

Mehta, K., Bakulin, A., Sheiman, J., Calvert, R. & Snieder, R., 2007. Improving the virtual source method by wavefield separation, *Geophysics,* **72,** V79–V86.

Mehta, K., Sheiman, J., Snieder, R. & Calvert, R., 2008. Strenghtening the virtual-source method for time-lapse monitoring, *Geophysics,* **73,** S73–S80.

Meier, T., Lebedev, G., Nolet, G. & Dahlen, F.A., 1997. Diffraction tomography using multimode surface waves, *J. geophys. Res.,* **102,** 8255–8267.

Morse, P.F. & Hildebrandt, G.F., 1989. Ground-roll suppression by the stack array, *Geophysics,* **54,** 290–301.

Moschetti, M.P., Ritzwoller, M. & Shapiro, N., 2007. Surface wave tomography of the Western United States from ambient seismic noise: Rayleigh wave group velocity maps, *Geochem., Geophys., Geosys,* **8,** Q08010.

Özbek, A., 2000a. Adaptive beamforming with generalized linear constraints, *SEG Exp. Abs.,* **19,** 2081–2084.

Özbek, A., 2000b. Multichannel adaptive interference cancelling, *SEG Exp. Abs.,* **19,** 2088–2091.

Pedersen, H.A., Krüger, F. & the SVEKALAPKO Seismic Tomography Working Group, 2007. Influence of the seismic noise characteristics on noise correlations in the Baltic shield, *Geophys. J. Int.,* **168,** 197–210.

Regone, C.J., 1998. Suppression of coherent noise in 3-D seismology, *Leading Edge,* **17,** 1584–1589.

Rhie, J. & Romanowicz, B., 2004. Excitation of Earth's continuous free oscillations by atmosphere-ocean-seafloor coupling, *Nature,* **431,** 552–556.

Rhie, J. & Romanowicz, B., 2006. A study of the relation between ocean storms and the Earth's hum, *Geochem., Geophys., Geosys,* **7,** Q10004.

Ritzwoller, M., Shapiro, N., Barmin, M.P. & Levshin, A.L., 2002. Global surface wave diffraction tomography, *J. geophys. Res.,* **107,** 2335.

Ruigrok, E., Draganov, D. & Wapenaar, K., 2008. Global-scale seismic interferometry: theory and numerical examples, *Geophys. Prospect.,* **56,** 395–417.

Sabra, K.G., Roux, P. & Kuperman, W.A., 2005. Arrival-time structure of the time-averaged ambient noise cross-correlation function in an oceanic waveguide, *J. acoust. Soc. Am.,* **117,** 164–174.

Shapiro, N. & Campillo, M., 2004. Emergence of broadband Rayleigh waves from correlations of the ambient seismic noise, *Geophys. Res. Lett.,* **31,** L07614.

Shapiro, N., Campillo, M., Stehly, L. & Ritzwoller, M., 2005. High-resolution surface-wave tomography from ambient seismic noise, *Science,* **307,** 1615–1617.

Slob, E. & Wapenaar, K., 2007. Electromagnetic Green's functions retrieval by cross-correlation and cross-convolution in media with losses, *Geophys. Res. Lett.,* **34,** L05307-05301–L05307-05305.

Slob, E., Draganov, D. & Wapenaar, K., 2007. Interferometric electromagnetic Green's functions representations using propagation invariants, *Geophys. J. Int.,* **169,** 60–80.

Snieder, R., 1986. 3D Linearized scattering of surface waves and a

formalism for surface wave holography, *Geophys. J. R. astr. Soc.,* **84,** 581–605.
Snieder, R., 1988. The optical theorem for surface waves and the relation with surface wave attenuation, *Geophys. J.,* **95,** 293–302.
Snieder, R., 2002. Scattering of surface waves, in *Scattering and Inverse Scattering in Pure and Applied Science,* pp. 562–577, edsPike, R. & Sabatier, P., Academic Press, San Diego.
Snieder, R., 2004a. *A Guided Tour of Mathematical Methods for the Physical Sciences,* 2nd edn, Cambridge University Press, Cambridge.
Snieder, R., 2004b. Extracting the Green's function from the correlation of coda waves: a derivation based on stationary phase, *Phys. Rev. E,* **69,** 046610.
Snieder, R., 2007. Extracting the Green's function of attenuating heterogeneous media from uncorrelated waves, *J. acoust. Soc. Am.,* **121,** 2637–2643.
Snieder, R. & Nolet, G., 1987. Linearized scattering of surface waves on a spherical Earth, *J. Geophys.,* **61,** 55–63.
Snieder, R., Wapenaar, K. & Larner, K., 2006. Spurious multiples in seismic interferometry of primaries, *Geophysics,* **71,** SI111–SI124.
Snieder, R., van Wijk, K., Haney, M. & Calvert, R., 2008. The cancellation of spurious arrivals in Green's function extraction and the generalized optical theorem, *Phys. Rev. E,* **78,** 036606.
Spetzler, J. & Snieder, R., 2001. The effect of small-scale heterogeneity on the arrival time of waves, *Geophys. J. Int.,* **145,** 786–796.
Spetzler, J., Trampert, J. & Snieder, R., 2002. The effect of scattering in surface wave tomography, *Geophys. J. Int.,* **149,** 755–767.
Stehly, L., Campillo, M. & Shapiro, N., 2006. A study of the seismic noise from its long-range correlation properties, *J. Geophys. Res.,* **111,** B10306.
Steiner, B., Saenger, E.H. & Schmalholz, S.M., 2008. Time reverse modeling of low-frequency mircotremors: application to hydrocarbon reservoir localization, *Geophys. Res. Lett.,* **35,** L03307.
van Manen, D.-J., Robertsson, J.O.A. & Curtis, A., 2005. Modeling of wave propagation in inhomogeneous media, *Phys. Rev. Lett.,* **94,** 164301–164304.
van Manen, D.-J., Curtis, A. & Robertsson, J.O.A., 2006. Interferometric modeling of wave propagation in inhomogeneous elastic media using time reversal and reciprocity, *Geophysics,* **71,** SI47–SI60.
Vasconcelos, I.R., 2007. Interferometry in perturbed media, *PhD thesis*. Colorado School of Mines.
Vasconcelos, I.R. & Snieder, R., 2008a. Interferometry by deconvolution, part 2: theory for elastic waves and application to drill-bit seismic imaging, *Geophysics,* **73,** S129–S141.
Vasconcelos, I.R. & Snieder, R., 2008b. Interferometry by deconvolution, part 1: theory for acoustic waves and numerical examples, *Geophysics,* **73,** S115–S128.
Wang, Y., 2002. A stable and efficient approach of inverse-*Q* filtering, *Geophysics,* **67**.
Wapenaar, K., 2004. Retrieving the elastodynamic Green's function of an arbitrary inhomogeneous medium by cross correlation, *Phys. Rev. Lett.,* **93,** 254301–254304.
Wapenaar, K., 2007. General representations for wavefield modeling and inversion in geophysics, *Geophysics,* **72,** SM5–SM17.
Wapenaar, K. & Fokkema, J., 2006. Green's function representations for seismic interferometry, *Geophysics,* **71,** SI33–SI44.
Weaver, R.L. & Lobkis, O.I., 2001. On the emergence of the Green's function in the correlations of a diffuse field, *J. acoust. Soc. Am.,* **110,** 3011–3017.
Wapenaar, K., Thorbecke, J. & Draganov, D., 2004. Relations between reflection and transmission responses of three-dimensional inhomogeneous media, *Geophys. J. Int.,* **156,** 179–194.
Wapenaar, K., Slob, E. & Snieder, R., 2008. Seismic and electromagnetic controlled-source interferometry in dissipative media, *Geophys. Prospect.,* **56,** 419–434.
Yang, Y., Ritzwoller, M., Levshin, A.L. & Shapiro, N., 2007. Ambient noise Rayleigh wave tomography across Europe, *Geophys. J. Int.,* **168,** 259–274.

APPENDIX A: STATIONARY PHASE EVALUATION FOR SINGLE-SCATTERED SURFACE WAVES

Halliday & Curtis (2009) use seismic interferometry, stationary-phase analysis and scattered surface wave Green's functions to derive a generalized optical theorem for surface waves. This theorem correctly describes the amplitude and phase relationship between incident and scattered surface wave modes from scatterers at any depth in a layered medium. The analysis that they present not only has implications for general scattering of surface waves, but there are also insights that can be gained regarding the application of seismic interferometry to scattered surface waves. For the readers convenience, we first review the stationary-phase analysis of Halliday & Curtis (2009). Rather than simply re-deriving their generalized optical theorem, we consider the role of each of the terms in the analysis of seismic interferometry for scattered surface waves before deriving the optical theorem for the specific case of isotropic point scatterers corresponding to density perturbations. This allows us to derive constraints on the real and imaginary parts of the scattering amplitudes, which allow us to calculate singly and multiply scattered surface waves efficiently. The stationary-phase analysis we consider is an extension of the work of Halliday & Curtis (2008) to scattered surface waves. The results of this analysis are discussed in detail in Section 2 of the main text.

To solve eq. (1) for scattered surface waves, we require appropriate Green's functions. Following Snieder (2002), the single (point) scattered surface wave field, $u_i^{(1)}(\mathbf{r}_\mathrm{B}, \omega)$ at a location $\mathbf{r}_\mathrm{B}$ due to an incident wavefield generated by a point force in the m direction at location $\mathbf{r}_\mathrm{A}$ is

$$u_i^{(1)}(\mathbf{r}_\mathrm{B}, \omega) = \sum_{\sigma\nu} p_i^{\sigma}(z_\mathrm{B}, \varphi_{0\mathrm{B}}) \frac{\mathrm{e}^{\mathrm{i}(k_\sigma X_{0\mathrm{B}} + \frac{\pi}{4})}}{\sqrt{\frac{\pi}{2} k_\sigma X_{0\mathrm{B}}}} V^{\sigma\nu}(\varphi_{0\mathrm{B}}, \varphi_{\mathrm{A}0}) \frac{\mathrm{e}^{\mathrm{i}(k_\nu X_{\mathrm{A}0} + \frac{\pi}{4})}}{\sqrt{\frac{\pi}{2} k_\nu X_{\mathrm{A}0}}} p_m^{\nu *}(z_\mathrm{A}, \varphi_{\mathrm{A}0}), \tag{A1}$$

where $\mathbf{r}_0$ is the scattering location, $V^{\sigma\nu}(\varphi_{0\mathrm{B}}, \varphi_{\mathrm{A}0})$ is the scattering matrix for an incident wave with azimuth $\varphi_{\mathrm{A}0}$ and a scattered wave with azimuth $\varphi_{0\mathrm{B}}$, k_ν is the wavenumber associated with the νth surface wave mode, $X_{\mathrm{A}0}$ and $X_{0\mathrm{B}}$ are the horizontal offsets between the scatterer at $\mathbf{r}_0$ and locations $\mathbf{r}_\mathrm{A}$ and $\mathbf{r}_\mathrm{B}$ respectively, $\varphi_{\mathrm{A}0}$ and $\varphi_{0\mathrm{B}}$ are the azimuth of the horizontal paths between $\mathbf{r}_\mathrm{A}$ and the scatterer at $\mathbf{r}_0$ and between the scatterer at $\mathbf{r}_0$ and $\mathbf{r}_\mathrm{B}$ respectively, and z_A and z_B are the depths of $\mathbf{r}_\mathrm{A}$ and $\mathbf{r}_\mathrm{B}$, respectively (Fig. 20). To simplify the expression the modal normalization $8c^\nu U^\nu I_1^\nu = 1$ is assumed (Snieder 2002), where c^ν, U^ν and I_1^ν are, retrospectively, the phase velocity, group velocity and kinetic energy for the current mode and p_i^ν is the ith component of the polarization vector

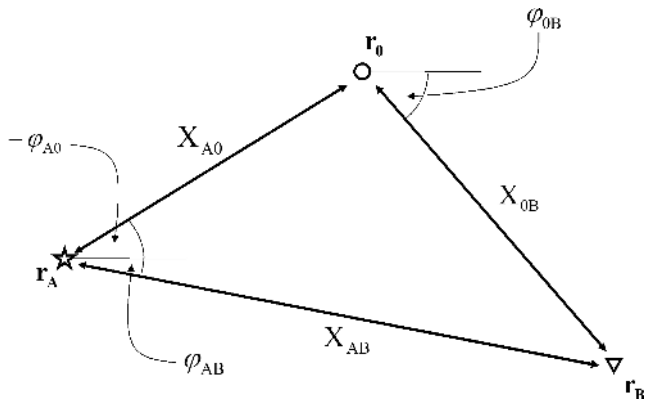

Figure 20. Geometric variables used to describe the scattered surface wave Green's function.

$$\mathbf{p}^{\nu}(z,\varphi)=\begin{pmatrix} r_1^{\nu}(z)\cos\varphi \\ r_1^{\nu}(z)\sin\varphi \\ ir_2^{\nu}(z)\end{pmatrix}, \tag{A2}$$

where $r_1^{\nu}(z)$ and $r_2^{\nu}(z)$ are the horizontal and vertical Rayleigh-wave eigenfunctions, respectively. This wavefield representation is for a single frequency, and in the following, we assume summation over the relevant frequency range.

The incident wavefield $u_i^{(0)}(\mathbf{r}_B,\omega)$ due to the same source at location $\mathbf{r}_A$ is

$$u_i^{(0)}(\mathbf{r}_B,\omega)=\sum_{\nu} p_i^{\nu}(z_B,\varphi_{AB})p_m^{\nu *}(z_A,\varphi_{AB})\frac{e^{i(k_\nu X_{AB}+\frac{\pi}{4})}}{\sqrt{\frac{\pi}{2}k_\nu X_{AB}}}, \tag{A3}$$

where X_{AB} and φ_{AB} are the offset and azimuth describing the horizontal projection of the path between $\mathbf{r}_A$ and $\mathbf{r}_B$ (Fig. 20).

The particle-displacement Green's function due to a point force is then the sum of the incident and scattered wavefield:

$$\begin{aligned} G_{im}(\mathbf{r}_B,\mathbf{r}_A)=&\sum_{\nu} p_i^{\nu}(z_B,\varphi_{AB})p_m^{\nu *}(z_A,\varphi_{AB})\frac{e^{i(k_\nu X_{AB}+\frac{\pi}{4})}}{\sqrt{\frac{\pi}{2}k_\nu X_{AB}}} \\ &+\sum_{\sigma\nu} p_i^{\sigma}(z_B,\varphi_{0B})\frac{e^{i(k_\sigma X_{0B}+\frac{\pi}{4})}}{\sqrt{\frac{\pi}{2}k_\sigma X_{0B}}}V^{\sigma\nu}(\varphi_{0B},\varphi_{A0})\frac{e^{i(k_\nu X_{A0}+\frac{\pi}{4})}}{\sqrt{\frac{\pi}{2}k_\nu X_{A0}}}p_m^{\nu *}(z_A,\varphi_{A0}), \end{aligned} \tag{A4}$$

and the particle-displacement deformation-rate Green's function is

$$\begin{aligned} n_j c_{njkm}\partial_k G_{im}(\mathbf{r}_B,\mathbf{r}_A)=&\sum_{\nu} p_i^{\nu}(z_B,\varphi_{AB})T_m^{\nu *}(z_A,\varphi_{AB})\frac{e^{i(k_\nu X_{AB}+\frac{\pi}{4})}}{\sqrt{\frac{\pi}{2}k_\nu X_{AB}}} \\ &+\sum_{\sigma\nu} p_i^{\sigma}(z_B,\varphi_{0B})\frac{e^{i(k_\sigma X_{0B}+\frac{\pi}{4})}}{\sqrt{\frac{\pi}{2}k_\sigma X_{0B}}}V^{\sigma\nu}(\varphi_{0B},\varphi_{A0})\frac{e^{i(k_\nu X_{A0}+\frac{\pi}{4})}}{\sqrt{\frac{\pi}{2}k_\nu X_{A0}}}T_m^{\nu *}(z_A,\varphi_{A0}), \end{aligned} \tag{A5}$$

where geometric variables are defined in Fig. 20, and T_n^{ν} is the nth component of the traction vector (Halliday & Curtis 2008, Appendix A)

$$\mathbf{T}^{\nu}(z,\varphi)=\begin{pmatrix} ik_\nu r_1^{\nu}(z)\cos^2\varphi & ik_\nu r_1^{\nu}(z)\cos\varphi\sin\varphi & -k_\nu r_2^{\nu}(z)\cos\varphi \\ ik_\nu r_1^{\nu}(z)\cos\varphi\sin\varphi & ik_\nu r_1^{\nu}(z)\sin^2\varphi & -k_\nu r_2^{\nu}(z)\sin\varphi \\ \frac{\partial}{\partial z}r_1^{\nu}(z)\cos\varphi & \frac{\partial}{\partial z}r_1^{\nu}(z)\sin\varphi & \frac{\partial}{\partial z}ir_2^{\nu}(z)\end{pmatrix} n_j c_{njkl}. \tag{A6}$$

Note that Halliday & Curtis (2009) consider a single incident surface wave mode and a single scattered surface wave mode. This is adequate to derive a generalized optical theorem that describes the scattering of a single incident and a single scattered mode. However, since we may wish to consider our analysis in terms of the application of seismic interferometry to multimode surface waves, we use a full sum over surface wave modes in our Green's functions.

Substitution of these Green's functions into eq. (1) results in four terms: the cross-correlation of the direct Rayleigh wave at one receiver with the direct Rayleigh wave at the other (*T1*); the cross-correlation of the direct Rayleigh wave at one receiver with the scattered surface wave at the other (*T2* and *T3*) and the cross-correlation of the scattered surface wave at one receiver with the scattered surface wave at the other (*T4*). We now consider each of these terms in turn.

To solve the interferometric integral using a stationary phase analysis we use a cylindrical co-ordinate system with the scatterer placed at radius equal to zero, and define the locations $\mathbf{r}_A$, $\mathbf{r}_B$, $\mathbf{r}_S$ and $\mathbf{r}_0$ as (Fig. 21)

$$\mathbf{r}_A=\begin{pmatrix} X_{A0}\cos(\varphi_{A0}+\pi) \\ X_{A0}\sin(\varphi_{A0}+\pi) \\ z_A\end{pmatrix},\quad \mathbf{r}_B=\begin{pmatrix} X_{0B}\cos\varphi_{0B} \\ X_{0B}\sin\varphi_{0B} \\ z_B\end{pmatrix},\quad \mathbf{r}_S=\begin{pmatrix} X_{S0}\cos(\varphi_{S0}+\pi) \\ X_{S0}\sin(\varphi_{S0}+\pi) \\ z_S\end{pmatrix},\quad \mathbf{r}_0=\begin{pmatrix} 0 \\ 0 \\ z_0\end{pmatrix}. \tag{A7}$$

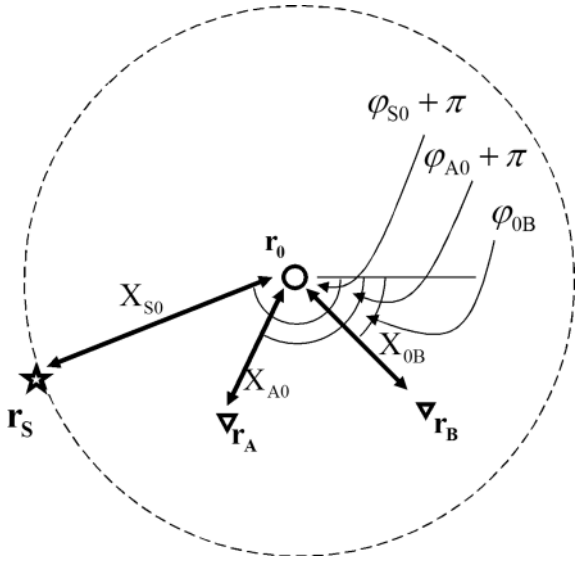

Figure 21. Sketch illustrating the geometry (in the horizontal plane) that is used in the stationary phase analysis. The scatterer $\mathbf{r}_0$ is placed at the centre of the coordinate system ($\mathbf{r} = 0$).

In the Green's functions (A4) and (A5), the terms such as X_{A0} and φ_{A0} describe the propagation path of the surface wave. The order of the subscripts identifies the direction of propagation, for example A0 denotes that these parameters describe the wave propagating from $\mathbf{r}_A$ to $\mathbf{r}_0$. For consistency, we have defined the vectors (A7) using the same notation as eqs (A1)–(A5). The cylindrical coordinate system is centred on the scatterer, and this requires that for the angles describing propagation 'toward' the scatterer we must add a factor π since all vectors are defined pointing 'away' from the scatterer.

A1 Term *T1*

T1 is the cross-correlation of the direct surface waves propagating in the background medium recorded at each receiver. The treatment of this term is exactly the same as the treatment of Rayleigh waves presented by Halliday and Curtis (2008). This results in the exact part of the Green's function for the direct surface wave (i.e. the wavefield in the homogeneous background medium).

A2 Terms *T2* and *T3*

Terms *T2* and *T3* are the cross-correlations of the direct surface wave at one receiver with the scattered surface wave at another (and vice verse), that is,

$$T2 = \sum_{\nu,\sigma\nu'} \int_S \frac{\mathrm{e}^{\mathrm{i}\left(-k_\nu X_{SA}+k_\sigma X_{0B}+k_{\nu'} X_{S0}+\frac{\pi}{4}\right)}}{\frac{\pi}{2}\sqrt{\frac{\pi}{2}k_\sigma k_{\nu'} k_\nu X_{SA} X_{0B} X_{S0}}} p_i^\sigma(z_B,\varphi_{0B}) p_m^{\nu *}(z_A,\varphi_{SA}) V^{\sigma\nu'}(\varphi_{0B},\varphi_{S0}) \times \left[p_n^{\nu' *}(z_S,\varphi_{S0}) T_n^\nu(z_S,\varphi_{SA}) - p_n^\nu(z_S,\varphi_{SA}) T_n^{\nu' *}(z_S,\varphi_{S0})\right] \mathrm{d}S. \quad \text{(A8)}$$

To analyse this integral we use the cylindrical coordinate system introduced above, and to find the stationary phase condition we need the lengths of each of the propagation paths. In cylindrical coordinates the length X_{SA} can be related to the other paths as follows:

$$X_{SA} = \sqrt{X_{S0}^2 - 2X_{S0}X_{A0}\cos(\varphi_{S0}-\varphi_{A0}) + X_{A0}^2}, \quad \text{(A9)}$$

where geometric variables are illustrated in (Fig. 21). To determine the stationary points of the integral we then require the first derivatives of X_{SA}, X_{S0}, X_{A0} and X_{0B} with respect to the integration direction. Since there is no dependence on z, we consider the φ_{S0}-derivatives using the geometry defined in (A7):

$$\frac{\partial X_{SA}}{\partial \varphi_{S0}} = \frac{X_{S0}X_{A0}}{X_{SA}} \sin(\varphi_{S0}-\varphi_{A0}), \quad \text{(A10)}$$

$$\frac{\partial X_{A0}}{\partial \varphi_{S0}} = 0, \quad \text{(A11)}$$

$$\frac{\partial X_{0B}}{\partial \varphi_{S0}} = 0, \quad \text{(A12)}$$

$$\frac{\partial X_{S0}}{\partial \varphi_{S0}} = 0. \tag{A13}$$

In the following analysis, we require stationary-phase conditions for integration in the φ_{S0}-direction. The integral *T2* is stationary when,

$$\frac{\partial X_{S0}}{\partial \varphi_{S0}} = \frac{\partial X_{SA}}{\partial \varphi_{S0}}, \tag{A14}$$

that is,

$$0 = \sin(\varphi_{S0} - \varphi_{A0}) \tag{A15}$$

that is, the stationary-phase conditions are $(\varphi_{S0} - \varphi_{A0}) = 0$ and $(\varphi_{S0} - \varphi_{A0}) = \pi$.

We use $\varphi_{S0} = \varphi_{SA}$ at the stationary point, and from Halliday & Curtis (2008), we can solve the depth dependant part of the integral using,

$$\int_0^\infty p_n^{\nu *}(z_S, \varphi_{S0}) T_n^{\nu}(z_S, \varphi_{S0}) - p_n^{\nu}(z_S, \varphi_{S0}) T_n^{\nu *}(z_S, \varphi_{S0}) \mathrm{d}z$$
$$= \frac{1}{2} i k_\nu (\cos\varphi_{S0} n_x + \sin\varphi_{S0} n_y), \tag{A16}$$

where the terms with $\nu \neq \nu'$ have been cancelled by the Rayleigh-wave orthogonality relationship (Halliday & Curtis, 2008). If we allow the integration surface to be a cylinder with extremely large radius such that $\cos\varphi_{S0} = -n_x$ and $\sin\varphi_{S0} = -n_y$,

$$\int_0^\infty p_n^{\nu *}(z_S, \varphi_{S0}) T_n^{\nu}(z_S, \varphi_{S0}) - p_n^{\nu}(z_S, \varphi_{S0}) T_n^{\nu *}(z_S, \varphi_{S0}) \mathrm{d}z = -\frac{1}{2} \mathrm{i} k_\nu. \tag{A17}$$

Using this relationship and $\mathrm{d}S = X_{S0}\, \mathrm{dz}\, \mathrm{d}\varphi_{S0}$ we find,

$$T2 = -\frac{\mathrm{i}k_\nu}{\pi} \sum_{\sigma\nu} \int_S \frac{\mathrm{e}^{\mathrm{i}\left(-k_\nu X_{SA} + k_\sigma X_{0B} + k_\nu X_{S0} + \frac{\pi}{4}\right)}}{k_\nu \sqrt{\frac{\pi}{2} k_\sigma X_{SA} X_{0B} X_{S0}}} p_i^{\sigma}(z_B, \varphi_{0B}) p_m^{\nu *}(z_A, \varphi_{SA}) V^{\sigma\nu}(\varphi_{0B}, \varphi_{S0}) X_{S0} \mathrm{d}\varphi_{S0}. \tag{A18}$$

We now wish to solve the integral,

$$I2 = \int_S \frac{\mathrm{e}^{\mathrm{i}\left(-k_\nu X_{SA} + k_\sigma X_{0B} + k_\nu X_{S0} + \frac{\pi}{4}\right)}}{k_\nu \sqrt{\frac{\pi}{2} k_\sigma X_{SA} X_{0B} X_{S0}}} V^{\sigma\nu}(\varphi_{0B}, \varphi_{S0}) X_{S0} \mathrm{d}\varphi_{S0,} \tag{A19}$$

using the method of stationary phase. This requires the second derivatives of X_{SA} and X_{S0} at the stationary point [i.e. when $0 = \sin(\varphi_{S0} - \varphi_{A0})$],

$$\frac{\partial^2 X_{SA}}{\partial \varphi_{S0}^2} = \frac{X_{S0} X_{A0} \cos(\varphi_{S0} - \varphi_{A0})}{\sqrt{X_{S0}^2 - 2 X_{S0} X_{A0} \cos(\varphi_{S0} - \varphi_{A0}) + X_{A0}^2}}, \tag{A20}$$

and

$$\frac{\partial^2 X_{S0}}{\partial \varphi_{S0}^2} = 0. \tag{A21}$$

At the first stationary point ($\varphi_{S0} - \varphi_{A0} = 0$), eq. (A20) becomes

$$\frac{\partial^2 X_{SA}}{\partial \varphi_{S0}^2} = \frac{X_{S0} X_{A0}}{X_{SA}}, \tag{A22}$$

since at this stationary point, $X_{SA} = X_{S0} - X_{A0}$ (Fig. 4a). At the second stationary point $\varphi_{S0} - \varphi_{A0} = \pi$ and $X_{SA} = X_{S0} + X_{A0}$ (Fig. 4b); so,

$$\frac{\partial^2 X_{SA}}{\partial \varphi_{S0}^2} = \frac{-X_{S0} X_{A0}}{X_{SA}}. \tag{A23}$$

We first evaluate the stationary point $\varphi_{S0} - \varphi_{A0} = 0$. Following Snieder (2004b), the solution to the integral is,

$$I2 = \frac{\mathrm{e}^{\mathrm{i}\left(-k_\nu X_{SA} + k_\sigma X_{0B} + k_\nu X_{S0} + \frac{\pi}{4}\right)}}{k_\nu \sqrt{\frac{\pi}{2} k_\sigma X_{SA} X_{0B} X_{S0}}} \mathrm{e}^{-\mathrm{i}\pi/4} \sqrt{\frac{2\pi}{k_\nu}} \frac{X_{S0}}{\sqrt{\frac{X_{S0} X_{A0}}{X_{SA}}}} V^{\sigma\nu}(\varphi_{0B}, \varphi_{S0}) \tag{A24}$$

$$= \frac{2}{k_\nu} \frac{\mathrm{e}^{\mathrm{i}(-k_\nu X_{SA} + k_\sigma X_{0B} + k_\nu X_{S0})}}{\sqrt{k_\sigma k_\nu X_{0B} X_{A0}}} V^{\sigma\nu}(\varphi_{0B}, \varphi_{S0}). \tag{A25}$$

Substituting *I2* into eq. (A18), we obtain

$$T2_p = -\frac{2\mathrm{i}}{\pi} \sum_{\sigma\nu} \frac{\mathrm{e}^{\mathrm{i}(-k_\nu X_{SA} + k_\sigma X_{0B} + k_\nu X_{S0})}}{\sqrt{k_\sigma k_\nu (X_{0B} X_{A0})}} p_i^{\sigma}(z_B, \varphi_{0B}) p_m^{\nu *}(z_A, \varphi_{SA}) V^{\sigma\nu}(\varphi_{0B}, \varphi_{S0}), \tag{A26}$$

where the subscript p indicates that this is a physical term. If $\varphi_{S0} - \varphi_{A0} = 0$ then $X_{SA} = X_{S0} - X_{A0}$ and $\varphi_{S0} = \varphi_{SA} = \varphi_{A0}$, so the integral becomes,

$$T2_p = -\sum_{\sigma\nu} \frac{e^{i\left(k_\nu X_{A0} + k_\sigma X_{0B} + \frac{\pi}{2}\right)}}{\frac{\pi}{2}\sqrt{k_\sigma k_\nu (X_{0B} X_{A0})}} p_i^\sigma(z_B, \varphi_{0B}) p_m^{\nu *}(z_A, \varphi_{A0}) V^{\sigma\nu}(\varphi_{0B}, \varphi_{A0}). \tag{A27}$$

Thus, term *T2* provides the correct causal scattered surface wave as desired (*cf.* the second term of eq. A4). Following a similar process for the second stationary point (when $\varphi_{S0} - \varphi_{A0} = \pi$, $X_{SA} = X_{S0} + X_{A0}$ and $\varphi_{S0} = \varphi_{SA} = \varphi_{A0} + \pi$), the integral becomes

$$T2_{np} = -\sum_{\sigma\nu} \frac{e^{i(k_\sigma X_{0B} - k_\nu X_{A0})}}{\frac{\pi}{2}\sqrt{k_\sigma k_\nu (X_{A0} X_{0B})}} p_i^\sigma(z_B, \varphi_{0B}) p_m^{\nu *}(z_A, \varphi_{A0} + \pi) V^{\sigma\nu}(\varphi_{0B}, \varphi_{A0} + \pi). \tag{A28}$$

This term does not correspond to any part of the Green's function defined in eq. (A4)—subscript np indicates that this is a non-physical arrival. Thus we show that term *T2* introduces a spurious arrival. Note that if we reverse the order of cross-correlation (i.e. use the direct surface wave at $\mathbf{r}_B$ and the scattered surface wave at $\mathbf{r}_A$) and repeat the above process to analyse contribution *T3*, we find that the two terms are equal to

$$T3_p = \sum_{\sigma\nu} \frac{e^{-i\left(k_\nu X_{A0} + k_\sigma X_{0B} + \frac{\pi}{2}\right)}}{\frac{\pi}{2}\sqrt{k_\sigma k_\nu (X_{A0} X_{0B})}} p_i^{\sigma *}(z_B, \varphi_{0B}) p_m^{\nu}(z_A, \varphi_{A0}) V^{\sigma\nu *}(\varphi_{0B}, \varphi_{A0}), \tag{A29}$$

and for the second term

$$T3_{np} = \sum_{\sigma\nu} \frac{e^{i(k_\sigma X_{0B} - k_\nu X_{A0})}}{\frac{\pi}{2}\sqrt{k_\sigma k_\nu (X_{A0} X_{0B})}} p_i^{\sigma *}(z_B, \varphi_{0B}) p_m^{\nu}(z_A, \varphi_{A0} + \pi) V^{\sigma\nu *}(\varphi_{0B}, \varphi_{A0} + \pi), \tag{A30}$$

see Figs 4(c) and (d). Again by comparing with eq. (A4), we see that $T3_p$ contributes the true scattered surface wave event but in the time-reversed part of the interferometric integral due to the complex conjugation of eq. (A29) with respect to the second term in eq. (A4). $T3_{np}$, on the other hand, contributes a non-physical arrival with the same phase as $T2_{np}$ but with opposite sign and complex conjugation of the scattering matrix. Note that if the scattering matrix is real, as is the case in a Born analysis, then $T2_{np}$ and $T3_{np}$ provide mutually cancelling terms. However, if we wish to consider higher order terms, we must also consider the non-linear feedback of the scatterer on the propagating wavefield. By higher order, we refer to any part of the wavefield that has been influenced by scatterers more than once. We consider term *T4* to be a higher order term, as even though this is a single-scattering example, term *T4* involves the cross-correlation of two scattered waves; although it would not normally be considered during a Born analysis, we now show the importance of this higher order term in seismic interferometry of single-scattered waves.

A3 Term *T4*

Term *T4* is the cross-correlation of the scattered surface waves recorded at both receivers:

$$\begin{aligned} T4 = \sum_{\sigma\nu,\sigma'\nu'} \int_S & \frac{e^{i\left(-k_\sigma X_{A0} - k_\nu X_{S0} + k_{\sigma'} X_{0B} + k_{\nu'} X_{S0}\right)}}{\frac{\pi^2}{4}\sqrt{k_\sigma k_\nu k_{\sigma'} k_{\nu'} X_{S0} X_{A0} X_{S0} X_{0B}}} \\ & \times p_i^\sigma(z_B, \varphi_{0B}) p_m^{\sigma' *}(z_A, \varphi_{A0} + \pi) V^{\sigma\nu}(\varphi_{0B}, \varphi_{S0}) V^{\sigma'\nu' *}(\varphi_{A0} + \pi, \varphi_{S0}) \\ & \times \left(p_n^{\nu *}(z_S, \varphi_{S0}) T_n^{\nu'}(z_S, \varphi_{S0}) - p_n^{\nu'}(z_S, \varphi_{S0}) T_n^{\nu *}(z_S, \varphi_{S0})\right) \mathrm{d}S. \end{aligned} \tag{A31}$$

Note that the incident wavefield upon the scatterer is the same for both receiver positions. Again, using the Rayleigh wave orthogonality relationship and expression (A17), we find,

$$\begin{aligned} T4 = -\sum_{\sigma,\sigma'\nu} \frac{2i}{\pi^2} \int_S & \frac{e^{i(-k_\sigma X_{A0} + k_\sigma X_{0B})}}{X_{S0}\sqrt{k_\sigma k_{\sigma'} X_{A0} X_{0B}}} \\ & \times p_i^\sigma(z_B, \varphi_{0B}) p_m^{\sigma' *}(z_A, \varphi_{A0} + \pi) V^{\sigma\nu}(\varphi_{0B}, \varphi_{S0}) V^{\sigma'\nu *}(\varphi_{A0} + \pi, \varphi_{S0}) \, \mathrm{d}S, \end{aligned} \tag{A32}$$

where we use the same constraints on the boundary as when evaluating terms *T2* and *T3* (i.e. a cylinder with large radius centred on the scatterer). Since this term is always stationary each source location provides a contribution to the interferometric integral and does not cancel. To solve the entire interferometric integral (i.e. including both first-order terms like *T2* and higher order terms like *T4*) we must consider the non-linear feedback of the scatterer on the propagating wavefield.

To do this, we require an optical theorem for surface waves, originally formulated by Snieder (1988), who related the imaginary part of the scattering amplitude to the total scattered power, and further developed by Brandenburg & Snieder (1989) who investigate the attenuation of surface waves due to scattering. The optical theorem can be used to derive constraints on the real and imaginary parts of scattering amplitudes (e.g. as derived for 2-D acoustic scattering by Groenenboom & Snieder 1995). We use our interferometric analysis to derive constraints on the real and imaginary parts of the scattering amplitude for surface waves. Although similar results have been derived for various types of media, the result for surface waves is new. We show that this allows us to account for terms $T2_{np}$, $T3_{np}$ and *T4*. In the main text we use this condition to compute realistic scattered surface waves within the optical theorem.

We treat the special case where there are no conversions between different surface wave modes (i.e. $\sigma = \sigma' = \nu$) and define a complex scattering amplitude $V(\varphi_{0\mathrm{B}}, \varphi_{\mathrm{A}0})$,

$$V(\varphi_{0\mathrm{B}}, \varphi_{\mathrm{A}0}) = \mathrm{Re}V(\varphi_{0\mathrm{B}}, \varphi_{\mathrm{A}0}) + \mathrm{i} * \mathrm{Im}V(\varphi_{0\mathrm{B}}, \varphi_{\mathrm{A}0}). \tag{A33}$$

If we insert this scattering amplitude into eqs (A27) and (A29) it is clear that the correct scattered surface wave is recovered. However, inserting this into eqs (A28) and (A30) results in a non-cancelling term:

$$T2_{np} = \mathrm{i}\frac{\mathrm{e}^{\mathrm{i}\left(k_\nu X_{0\mathrm{B}} - k_\nu X_{\mathrm{A}0} + \frac{\pi}{2}\right)}}{\frac{\pi}{2}\sqrt{k_\nu k_\nu \left(X_{\mathrm{A}0} X_{0\mathrm{B}}\right)}} p_i^\nu(z_\mathrm{B}, \varphi_{0\mathrm{B}}) p_m^{\nu^*}(z_\mathrm{A}, \varphi_{\mathrm{A}0} + \pi) \left[\mathrm{Re}\, V(\varphi_{0\mathrm{B}}, \varphi_{\mathrm{A}0} + \pi) + \mathrm{i} * \mathrm{Im}V(\varphi_{0\mathrm{B}}, \varphi_{\mathrm{A}0} + \pi)\right], \tag{A34}$$

$$T3_{np} = -\mathrm{i}\frac{\mathrm{e}^{\mathrm{i}\left(k_\nu X_{0\mathrm{B}} - k_\nu X_{\mathrm{A}0} + \frac{\pi}{2}\right)}}{\frac{\pi}{2}\sqrt{k_\nu k_\nu \left(X_{0\mathrm{B}} X_{\mathrm{A}0}\right)}} p_i^{\nu^*}(z_\mathrm{B}, \varphi_{0\mathrm{B}}) p_m^\nu(z_\mathrm{A}, \varphi_{\mathrm{A}0} + \pi) \left[\mathrm{Re}\, V(\varphi_{0\mathrm{B}}, \varphi_{\mathrm{A}0} + \pi) - \mathrm{i} * \mathrm{Im}V(\varphi_{0\mathrm{B}}, \varphi_{\mathrm{A}0} + \pi)\right], \tag{A35}$$

Assuming that $i = m = 3$ the non-physical parts of terms *T2* and *T3* can be combined into a single term (T_{np}),

$$T_{np} = -2\mathrm{i}\frac{\mathrm{e}^{\mathrm{i}(k_\nu X_{0\mathrm{B}} - k_\nu X_{\mathrm{A}0})}}{\frac{\pi}{2}\sqrt{k_\nu k_\nu \left(X_{0\mathrm{B}} X_{\mathrm{A}0}\right)}} \mathrm{Im}V(\varphi_{0\mathrm{B}}, \varphi_{\mathrm{A}0} + \pi) p_3^\nu(z_\mathrm{B}, \varphi_{0\mathrm{B}}) p_3^{\nu^*}(z_\mathrm{A}, \varphi_{\mathrm{A}0} + \pi). \tag{A36}$$

To derive the constraints that the optical theorem places on the real and imaginary parts of the scattering amplitude we consider the forward scattering amplitude (Snieder 1988; Groenenboom & Snieder 1995). To do this we assume that geometries are chosen such that $\varphi_{0\mathrm{B}} = \varphi_{\mathrm{A}0} + \pi$, that is,

$$T_{np} = -2\mathrm{i}\frac{\mathrm{e}^{\mathrm{i}(k_\nu X_{0\mathrm{B}} - k_\nu X_{\mathrm{A}0})}}{\frac{\pi}{2}\sqrt{k_\nu k_\nu \left(X_{0\mathrm{B}} X_{\mathrm{A}0}\right)}} \mathrm{Im}V(\varphi_{0\mathrm{B}}, \varphi_{0\mathrm{B}}) p_3^\nu(z_\mathrm{B}, \varphi_{0\mathrm{B}}) p_3^{\nu^*}(z_\mathrm{A}, \varphi_{\mathrm{A}0} + \pi), \tag{A37}$$

and

$$T4 = -\frac{2\mathrm{i}}{\pi^2}\int_S \frac{\mathrm{e}^{i(-k_\nu X_{\mathrm{A}0} + k_\nu X_{0\mathrm{B}})}}{X_{S0}\sqrt{k_\nu k_\nu X_{\mathrm{A}0} X_{0\mathrm{B}}}} p_3^\nu(z_\mathrm{B}, \varphi_{0\mathrm{B}}) p_3^{\nu^*}(z_\mathrm{A}, \varphi_{0\mathrm{B}}) \left|V(\varphi_{0\mathrm{B}}, \varphi_{S0})\right|^2 \mathrm{d}S \tag{A38}$$

It then follows, that for this scattered wavefield representation to be exact that T_{np} must be equal to *T4*, that is,

$$\begin{aligned} -2\mathrm{i}&\frac{\mathrm{e}^{\mathrm{i}(k_\nu X_{0\mathrm{B}} - k_\nu X_{\mathrm{A}0})}}{\frac{\pi}{2}\sqrt{k_\nu k_\nu \left(X_{0\mathrm{B}} X_{\mathrm{A}0}\right)}} \mathrm{Im}V(\varphi_{0\mathrm{B}}, \varphi_{0\mathrm{B}}) p_3^\nu(z_\mathrm{B}, \varphi_{0\mathrm{B}}) p_3^{\nu^*}(z_\mathrm{A}, \varphi_{\mathrm{A}0} + \pi) \\ &= \frac{2\mathrm{i}}{\pi^2}\int_S \frac{\mathrm{e}^{\mathrm{i}(-k_\nu X_{\mathrm{A}0} + k_\nu X_{0\mathrm{B}})}}{X_{S0}\sqrt{k_\nu k_\nu X_{\mathrm{A}0} X_{0\mathrm{B}}}} p_3^\nu(z_\mathrm{B}, \varphi_{0\mathrm{B}}) p_3^{\nu^*}(z_a, \varphi_{0\mathrm{B}}) \left|V(\varphi_{0\mathrm{B}}, \varphi_{S0})\right|^2 \mathrm{d}S. \end{aligned} \tag{A39}$$

Finally, we remove the resulting common terms from both sides of eq. (A40) then the part of this expression dependent on the differing receiver locations is removed, that is, the right hand side is now equivalent to the power of the scattered wave

$$-\frac{4\mathrm{i}}{\pi}\mathrm{Im}V(\varphi_{0\mathrm{B}}, \varphi_{0\mathrm{B}}) = \frac{2\mathrm{i}}{\pi^2}\int_S \frac{1}{X_{S0}} \left|V(\varphi_{0\mathrm{B}}, \varphi_{S0})\right|^2 \mathrm{d}S, \tag{A40}$$

and rearranging,

$$-\mathrm{Im}V(\varphi_{0\mathrm{B}}, \varphi_{0\mathrm{B}}) = \frac{1}{2\pi}\int_S \frac{1}{X_{S0}} \left|V(\varphi_{0\mathrm{B}}, \varphi_{S0})\right|^2 \mathrm{d}S, \tag{A41}$$

We can simplify this expression following the approach of Brandenburg & Snieder (1989). First we assume that the surface is a cylinder with extremely large radius. The length X_{S0} is then approximately equal for all points on the boundary, and the horizontal projection of the azimuth from each boundary position is approximately equal to the normal to the boundary. We then use that $\mathrm{d}S = \mathrm{d}r\mathrm{d}\phi$, where r is the radius of the cylinder and ϕ is the scattering angle ($\varphi_{0\mathrm{B}} - \varphi_{S0}$). There is no depth integration as we have already solved the depth dependent part of the integral and the integral then becomes

$$-\mathrm{Im}V(\varphi_{0\mathrm{B}}, \varphi_{0\mathrm{B}}) = \frac{1}{2\pi}\int_0^{2\pi} \left|V(\varphi_{0\mathrm{B}}, \varphi_{S0})\right|^2 \mathrm{d}\phi. \tag{A42}$$

The scattering amplitude for an isotropic density perturbation has two parts, one independent of scattering angle, and one dependent on the scattering angle (Snieder 2002, eq. (43)). To allow us to calculate synthetic seismograms (in a similar fashion to Groenenboom & Snieder 1995) we assume that $V(\varphi_{0\mathrm{B}}, \varphi_{S0})$ has the following form that is,

$$V(\varphi_{0\mathrm{B}}, \varphi_{S0}) = V_1(\varphi_{0\mathrm{B}}, \varphi_{S0}) + V_2(\varphi_{0\mathrm{B}}, \varphi_{S0}) \cos\phi. \tag{A43}$$

We split eq. (A42) into two parts, a non-angular dependent part and an angularly dependent part,

$$-\mathrm{Im}V_1(\varphi_{0\mathrm{B}}, \varphi_{0\mathrm{B}}) = \frac{1}{2\pi}\int_0^{2\pi} \mathrm{Re}V_1(\varphi_{0\mathrm{B}}, \varphi_{S0})^2 + \mathrm{Im}V_1(\varphi_{0\mathrm{B}}, \varphi_{S0})^2 \mathrm{d}\phi, \tag{A44}$$

and

$$-\mathrm{Im}V_2(\varphi_{0\mathrm{B}},\varphi_{0\mathrm{B}})\cos\phi = \frac{1}{2\pi}\int_0^{2\pi}\left(\mathrm{Re}V_2(\varphi_{0\mathrm{B}},\varphi_{\mathrm{S}0})^2+\mathrm{Im}V_2(\varphi_{0\mathrm{B}},\varphi_{\mathrm{S}0})^2\right)\cos^2\phi\,\mathrm{d}\phi. \tag{A45}$$

Evaluating the integrals we find that the optical theorem places the following constraints on these two parts of the scattering amplitude,

$$\mathrm{Re}V_1=\sqrt{-\mathrm{Im}V_1(1+\mathrm{Im}V_1)}, \tag{A46}$$

and

$$\mathrm{Re}V_2=\sqrt{-\mathrm{Im}V_2(2\cos\phi+\mathrm{Im}V_2)}. \tag{A47}$$

By equating the non-physical parts of terms *T2* and *T3* with *T4*, we have found the constraints that the optical theorem places on surface waves scattered by an isotropic density perturbation. This is a special case of the generalized optical theorem derived by Halliday & Curtis (2009). Therefore, by using eqs (A46) and (A47) we can be certain that interferometric estimates generated using eq. (1) are not affected by non-physical arrivals. Thus, provided scattering is governed by the optical theorem, we have solved the interferometric integral for singly scattered surface waves. The constraints that we derive are for waves excited by and observed using vertical point-force sources and vertical displacement, respectively. Similar constraints could be derived for different source and receiver components if required. In the main body of this paper, we use relationships (A46) and (A47) to calculate synthetic seismograms to illustrate our findings.

APPENDIX B: ALTERATIONS FOR CONVOLUTION INTERFEROMETRY

In the main text we discuss the application of convolution-type interferometry to scattered surface waves. In this appendix, we adapt our stationary-phase analysis to allow us to consider this convolution-type approach.

It is possible to derive a relationship similar to eq. (1) that uses cross-convolution in place of cross-correlation. This is done by using the reciprocity theorem of the convolution-type as the starting point in the interferometric derivation, as opposed to a reciprocity theorem of the correlation-type (Wapenaar 2007). This derivation is very similar to the derivations of van Manen *et al.* (2006) and Wapenaar & Fokkema (2006), but there is an additional constraint on the location of the two receivers. In this configuration, we must have one receiver located inside the source boundary and the second receiver located outside the boundary. In correlation-type interferometry, time-reversed wavefields are introduced due to the fact that cross-correlation requires complex conjugation (or time-reversal) of one of the inputs. Since wavefields cannot be time-reversed in the presence of attenuation, this places the constraint that the medium of interest must be non-attenuating. In convolution-type interferometry there is no complex-conjugation, hence no time-reversed wavefields are introduced and no constraints are placed on the attenuation of the medium. We can therefore expect this form of interferometry to be useful in the presence of strong attenuation.

Adapting the approach of Slob *et al.* (2007) for the elastic case, the equivalent convolution form of eq. (1) is found to be

$$G_{im}(\mathbf{r}_B,\mathbf{r}_A) = \int_{\mathbf{r}_S\in S}\left\{G_{in}(\mathbf{r}_\mathrm{B},\mathbf{r}_\mathrm{S})n_j c_{njkl}\partial_k G_{ml}(\mathbf{r}_\mathrm{A},\mathbf{r}_\mathrm{S})-n_j c_{njkl}\partial_k G_{il}(\mathbf{r}_\mathrm{B},\mathbf{r}_\mathrm{S})G_{mn}(\mathbf{r}_\mathrm{A},\mathbf{r}_\mathrm{S})\right\}\mathrm{d}S, \tag{B1}$$

where one of $\mathbf{r}_\mathrm{A}$ and $\mathbf{r}_\mathrm{B}$ is inside the volume S, and the other is outside the volume.

With this new configuration in mind, we can make appropriate alterations to the stationary phase analysis. The analysis is very similar to the approach of Halliday & Curtis (2008). It can be shown that the combination of the new stationary-phase condition and the convolution-type integral has the same result as the combination of the old stationary phase condition and the correlation type integral. We choose not to present this lengthy derivation and instead, proceed to investigate the differences in stationary-phase conditions and the consequences for estimation of surface waves.

For the stationary points there is a sign change in the phase term. For the direct surface waves the phase term (P) for correlation-type interferometry is

$$P=\mathrm{i}k_\nu(X_\mathrm{SA}-X_\mathrm{SB}), \tag{B2}$$

and by taking the first-order derivatives we find that the integral is stationary when (Snieder 2004b; Halliday & Curtis 2008)

$$\varphi_\mathrm{SA}=\varphi_\mathrm{SB}. \tag{B3}$$

When we consider convolution-type interferometry, there is no complex conjugation, and the phase term in the interferometric integral becomes

$$P=\mathrm{i}k_\nu(X_\mathrm{SA}+X_\mathrm{SB}), \tag{B4}$$

and it is easily shown that the integral becomes stationary when

$$\varphi_\mathrm{SA}=\varphi_\mathrm{SB}+\pi. \tag{B5}$$

The same alterations can be made for the integral for scattered surface waves. The stationary phase conditions change in the same way, that is, for the physical arrival the condition changes from $\varphi_{\mathrm{S}0}=\varphi_{\mathrm{A}0}$ in correlation-type interferometry (see eqs A14 and A15, Appendix A) to

$$\varphi_{\mathrm{S}0}=\varphi_{\mathrm{A}0}+\pi, \tag{B6}$$

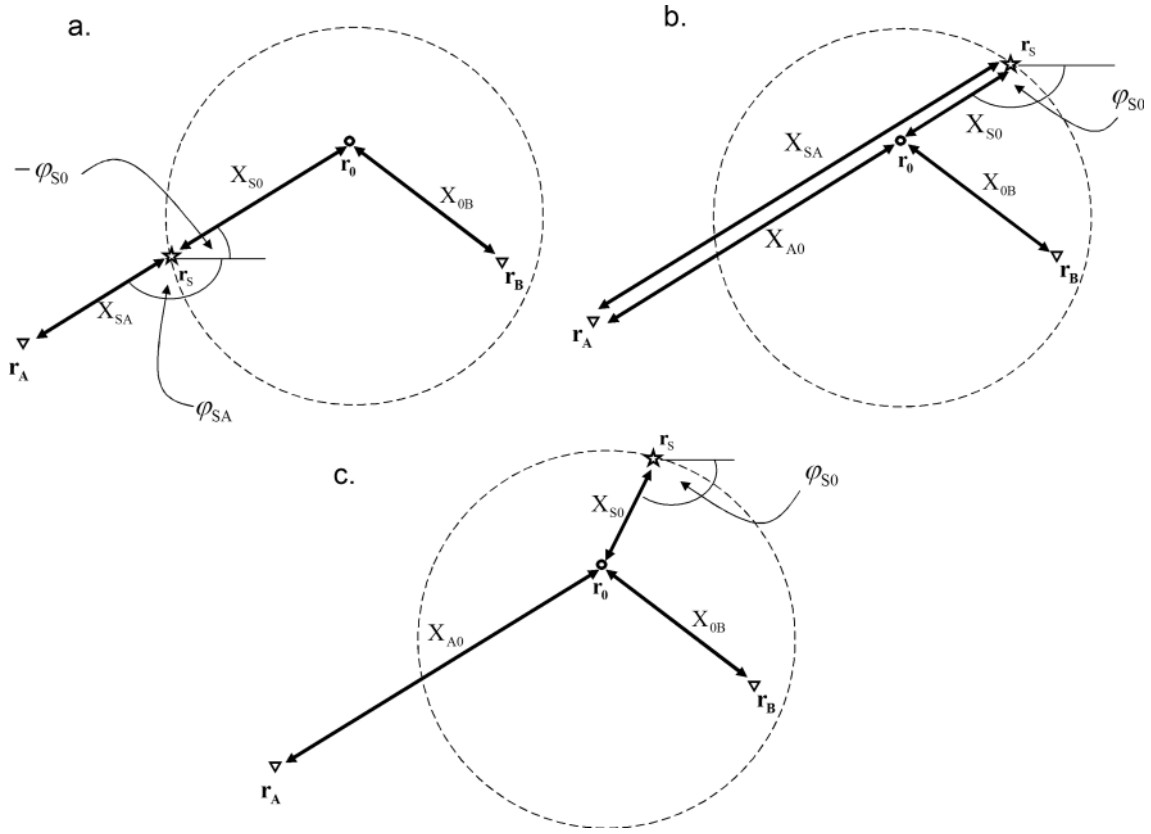

Figure 22. (a) Illustration of the stationary point for the scattered surface wave in convolution-type interferometry. (b) and (c) Corresponding geometries for the non-physical part of term *T2* (or *T3*) and Term *T4*, respectively.

For convolution-type interferometry, and for the non-physical stationary phase, the condition changes from $\varphi_{S0} = \varphi_{A0} + \pi$, for correlation-type interferometry to

$$\varphi_{S0} = \varphi_{A0},$$

for convolution-type interferometry. In Fig. 22(a) and (b), we show the geometries for this physical and non-physical stationary point, respectively. In Fig. 22(c), we also show the geometry corresponding to term *T4*.

Using the relationships $p_n^{\nu}(z, -\varphi) = p_n^{\nu *}(z, \varphi)$ and $T_n^{\nu}(z, -\varphi) = T_n^{\nu *}(z, \varphi)$. the stationary phase analysis is then the same as for the cross-correlation case. If we then consider the source terms for these contributions in the correlation case (e.g. eq. A16),

$$p_n^{\nu *}(z_S, \varphi_{S0}) T_n^{\nu}(z_S, \varphi_{S0}) - p_n^{\nu}(z_S, \varphi_{S0}) T_n^{\nu *}(z_S, \varphi_{S0}), \tag{B7}$$

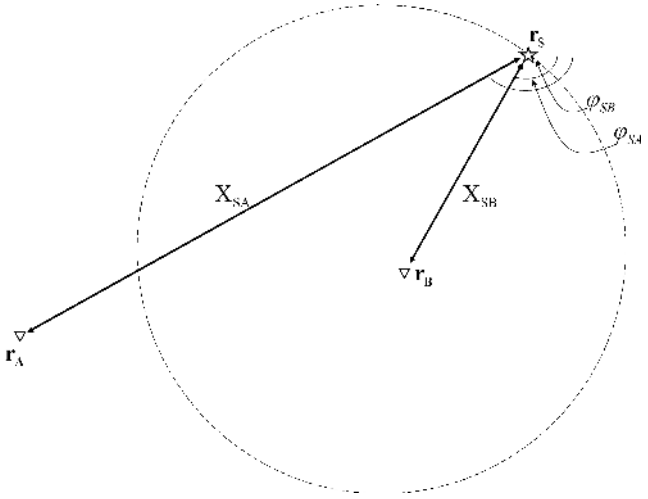

Figure 23. Sketch illustrating the geometry of the spurious stationary point arising in convolution-type interferometry.

we find that in the convolution case there is no complex conjugation:

$$p_n^v(z_S, \varphi_{S0})T_n^v(z_S, \varphi_{S0}) - p_n^v(z_S, \varphi_{S0})T_n^v(z_S, \varphi_{S0}) = 0. \tag{B8}$$

Hence term *T4* is equal to zero in convolution-type interferometry, and there are no non-physical arrivals. That is, despite being stationary, these points give a vanishing contribution to the interferometric integral. Hence there is no contribution from term *T4*, and terms *T2* and *T3* do not have any non-physical contributions and no mutually cancelling terms are introduced, the significance of which is discussed in Sections 3 and 4 of the main text.

However, there is one further contribution that we must consider. If we only have a boundary of sources at the surface, there is one point on the circle, which appears to be stationary. At this point, the sum of the offsets travelled between the source and receivers one and two is at its maximum, and therefore this looks like a stationary point (Fig. 23). However, this is not stationary—with a different shape of boundary this maximum value will occur at a different point because, in fact this point is non-stationary across a surface, but it is stationary along a line. We find that this event also cancels given integration with depth, similar to the cancellation of the cross-mode stationary points discussed by Halliday & Curtis (2008). This can be argued as follows: the Rayleigh-wave orthogonality relationship states that the time-domain product of different Rayleigh-wave modal solutions integrates to zero over depth. This holds for any pair of solutions to the Rayleigh-wave eigenvalue problem (and can also be shown to include solutions to the Love-wave eigenvalue problem). Since the convolved waves for this pseudo-stationary source point both travel along different azimuths, they can be considered as different solutions. Hence integration of their time-domain product over depth results in a value of zero.